CALICE Analysis Note CAN-049a
May, 2016

Comparison of Energy Reconstruction Schemes and Different Granularities in the CALICE AHCAL

The CALICE collaboration

Abstract

In this note, different energy reconstruction methods for the Analogue Hadronic Calorimeter (AHCAL) are compared. These methods were developed for the analogue, digital and semi-digital CALICE Hadronic Calorimeter physics prototypes and were used in analyses of data taken at various test beams.
The analogue data can also be processed in a way which emulates a digital readout system, thus the advantages and disadvantages of different energy reconstruction procedures can be studied using the same data sample. In this work this comparison is done by applying these procedures to AHCAL pion test beam data collected with the $1\,\mathrm{m}^3$ physics prototype with a granularity of 3×3 to $12 \times 12\,\mathrm{cm}^2$. The results were reproduced by means of GEANT4 based simulations. This confirms our understanding of the test beam and simulation setup. The simulation was also performed with cell sizes of $1 \times 1\,\mathrm{cm}^2$. The impact on the energy resolutions, using different reconstruction schemes will be discussed and compared to the digital and semi-digital HCAL prototype data.

This note contains preliminary CALICE results, and is for the use of members of the CALICE collaboration and others to whom permission has been given. [1]

[1]Corresponding author:
Coralie Neubüser; coralie.neubueser@desy.de

Contents

1 Introduction

For a future linear electron-positron collider like the International Linear Collider (ILC) or the Compact Linear Collider (CLIC), the desired jet energy resolution of 3–4 % for a wide range of jet energies can be achieved by using Particle Flow algorithms for the jet reconstruction. Within the CALICE collaboration, several concepts for a hadron calorimeter (HCAL) optimised for Particle Flow are studied and have been tested with $1\,\mathrm{m}^3$ large prototypes: the so-called analogue (A), digital (D) and semi-digital (SD) HCAL concepts [1]. The concepts differ in active material for the shower detection, granularity, readout technology and reconstruction method. This makes it difficult to disentangle the influence of each of these components to the energy resolution of jets as well as of individual particles. Since the AHCAL prototype has a larger cell size than the other two concepts, and the D- and SDHCAL prototypes do not provide analogue hit amplitude information, it is impossible to study all different aspects in test beam data. For the data taken with the AHCAL prototype, a direct comparison of the reconstruction procedures is possible, albeit with a cell size not optimal for the digital and semi-digital methods. The effect of the other differences can only be studied directly in simulation, where every aspect can be changed individually. For reliable results from the simulation it is important to validate the simulation of hadronic showers in the detector prototypes by comparing them to the measured test beam data.

In this note, pion test beam data taken with the AHCAL prototype are used to apply also the readout concepts and reconstruction procedures developed for the digital and semi-digital HCAL. The results are compared and the GEANT4 based simulation is validated. The validation confirmed the in-depth understanding of this technology and thus allowed a prediction for an AHCAL with $1 \times 1\,\mathrm{cm}^2$ granularity. The impact of the higher granularity on the different energy reconstruction schemes in terms of the resolution is discussed and compared to the test beam data of the S- and DHCAL.

2 Energy Reconstruction Procedures

For the three different CALICE Hadron Calorimeters, which use different active material and readout, three different energy reconstruction procedures were developed and are briefly described. In addition a new software compensation algorithm is developed and will be presented in the following.
This analysis studies the energy reconstruction of the AHCAL only, thus the recorded data of the ECAL and tail catcher muon tracker (TCMT), present in front and in the back of the AHCAL at the test beam, are not considered in the event by event energy reconstructions.

2.1 Analogue

The Analogue HCAL is a scintillator tile calorimeter with Silicon Photomultiplier (SiPM) read-out. Each tile is constituted by a square plastic scintillator with a wavelength-shifting fiber coupled to a SiPM. Within the scintillating plastic the charged particles excite the scintillator which emits photons. These photons are captured by the wavelength-shifting fibre that transports the light to the SiPM. A calibration is used to convert the measured ADC counts of the SiPM to the response of a muon or minimum-ionising particle (MIP) [2].
Within several test beam campaigns a $1\,\mathrm{m}^3$ physics prototype was tested and its single particle resolution was validated [3]. This prototype consists of up to 38 active layers interleaved with the steel absorber plates. The first 30 layers consist of tiles with three different tile sizes; 3×3, 6×6 and $12 \times 12\,\mathrm{cm}^2$, and the last 8 layers are assembled of 6×6 and $12 \times 12\,\mathrm{cm}^2$ tiles.
The visible signal $\mathrm{E_{sum}}$ for the reconstructed energy is calculated in units of MIP as a sum of cell signals above 0.5 MIP which are called hits. The 0.5 MIP threshold is used to reject noise. The MIP scale is converted to a GeV scale using an electromagnetic calibration factor ω which was determined from dedicated positron runs [4].
The scintillator-steel AHCAL is a non-compensating calorimeter, as its response to electrons is by a factor of $\mathrm{e}/\pi = 1.19$ higher than to pions of the same energy [3]. An additional scaling factor c is applied here to cover for the missing energy usually added from the TCMT [3]. This factor was estimated by fitting the mean analogue response with

$$\langle \mathrm{E_{sum}} \rangle = \frac{\mathrm{E_{beam}}}{\frac{\mathrm{e}}{\pi} \cdot \omega \cdot \mathrm{c}} \tag{1}$$

and found to be c = 1.04. Then the reconstructed energy in the AHCAL for each pion event is calculated from the measured energy E_{sum} [MIP] as follows:

$$E_{rec,AHCAL} = \frac{e}{\pi} \cdot \omega \cdot E_{sum} \cdot c \tag{2}$$

2.2 Digital

The Digital HCAL [5] is a sampling calorimeter with Resistive Plate Chamber (RPC) readout. A RPC consists of glass and a 1.15 mm gap filled with gas, read out by pad electrodes of $1 \times 1\,cm^2$ size placed on the back of the plates. The incoming particles traverse the gas and ionise it. The ionisation is amplified through avalanche processes induced by the high bias voltage applied to the RPC. The charge multiplication is quenched by the high resistivity of the glass. If the charge exceeds the pad threshold of 20-700 fC a hit is measured [6].
The measurement observable is the total number of hits in the HCAL N_{hits}. There is no information about the signal size. A calibration is done by equalising the response to obtain a similar multiplicity and efficiency for muons (MIP) in every layer. More sophisticated calibration procedures are under investigation [7].
Within the energy reconstruction a correction for the non-linearity is applied. The non-linearity arises from multiple particles traversing the same pad, limited granularity and binary information. Several approaches have been developed to correct for this non-linearity. Here, a simple approach is followed by fitting the mean response versus beam energy E_{beam} with a power law as $\langle N_{hits} \rangle = a \cdot (E_{beam})^b$ and taking the extracted parameters a and b for the reconstruction as follows:

$$E_{rec,DHCAL} = \sqrt[b]{\frac{N_{hits}}{a}}. \tag{3}$$

2.3 Semi-Digital

The principle of the semi-digital HCAL is similar to digital HCAL, but with a 2-bit read-out. A large SDHCAL prototype has been realised with RPCs. In addition several MICROMEGAS layers have been tested. The granularity of the readout of these devices was also $1 \times 1\,cm^2$. The difference between both is the readout, while the calorimetric sampling is the same. The 2 bit readout encodes the information of 3 thresholds. This additional information compared to the DHCAL has the goal to

identify multiple particles contributing to the signal of a pad. First results of test beams of the RPC SDHCAL physics prototype are published [8].
We will follow the same procedure of energy reconstruction as the SDHCAL physics prototype here: Reconstructing the energy as a sum of the weighted number of hits for the 3 thresholds, $E_{rec,SD}$ can be written as a function of N_1, the number of hits above the first and below the second; N_2, the number of hits above the second below the third; and N_3, the number of hits above the third threshold:

$$E_{rec,SD} = \alpha N_1 + \beta N_2 + \gamma N_3, \tag{4}$$

with the weights α,β and γ in units of GeV. Hadronic showers change their structure and evolution with energy, which is taken into account by parameterising α,β and γ as second order polynomials of the total number of hits $N_{hits} = N_1 + N_2 + N_3$. To find the best parameterisation of these calibration coefficients, a χ^2-like function of the form

$$\chi^2 = \sum_{i=1}^{N} \frac{\left(E^i_{beam} - E^i_{rec}\right)^2}{E^i_{beam}}, \tag{5}$$

is minimised, where i runs over all events.

2.4 Analogue Software Compensation

The purpose of the technique introduced in the following is the compensation for the difference in energy response of the electromagnetic and hadronic components in pion showers. In contrast to the regular analogue reconstruction, software compensation techniques apply this correction for each event individually by weighting the hits depending on their initial energy content (e_j) and the total visible energy E_{sum}. In this way, hits of electromagnetic content that typically have a higher energy density, get weighted down, while the hadronic parts can be weighted up. A proof of principle has been shown in [3]. The algorithm developed for this study is geared to the semi-digital weight estimation. Contrary to the previous techniques, the weights for the reconstruction $\omega\left(e_j\right)$ are parametrised as second order polynomials of the total visible energy E_{sum}, which is directly proportional to the beam momentum. This method determines 8 weights for 8 hit energy ranges, which will be further discussed in Chapter 4.4. With the weight parametrisation a χ^2 function, see Equation 5, is minimised by using the same number of events per beam energy. The resulting

weights in units of $\frac{\mathrm{GeV}}{\mathrm{MIP}}$ are then used to reconstruct the energy for each event by

$$\mathrm{E_{rec,SC}} = \sum_{\mathrm{j=0}}^{\mathrm{N_{hits}}} \omega\left(\mathrm{e_j}, \mathrm{E_{sum}}\right) \cdot \mathrm{e_j}. \tag{6}$$

In this way the beam energy is used for the weight determination, while only the measured energy $\mathrm{E_{sum}}$ is needed for the energy reconstruction.
This software compensation algorithm uses analogue hit information and is therefore here called Analogue Software Compensation. For a digital or semi-digital Calorimeter a similar algorithm can be applied, using the number of neighbouring hits for an energy density estimate. Thus weights dependent on this different energy density definition can be applied and the resolution improved [9].

3 Data and Simulations

For this analysis the AHCAL test beam data from 2007 with steel absorber is chosen. The reason for this choice was the good understanding of the data, validated by several published CALICE analyses [2, 3, 10, 11].
The 2007 CERN test beam setup consisted of 30 layers of CALICE silicon-tungsten ECAL, 38 layers of the scintillator-steel analogue HCAL and 16 layers of the scintillator-steel tail catcher and muon tracker (TCMT). The ECAL was separated into three sections of different absorber thicknesses: 1.4, 2.8 and 4.2 mm (radiation lengths 0.4, 0.8 and 1.2 $\mathrm{X_0}$). The absorber thickness of the HCAL was $\sim$ 1.75 cm. A detailed description of the test beam setup can be found in [11].

3.1 Monte Carlo Simulations

The test beam runs are simulated using the software packages GEANT4 version 9.6 patch 1, MOKKA v08_02 and ILCSOFT v01_17_05, followed by the digitisation using calice_soft v04-08 with the conversion coefficients 846 keV/MIP and 15 % optical crosstalk between the AHCAL tiles. As the physics lists FTFP_BERT and QGSP_BERT from GEANT4 9.6 show best performance for hadrons [11], they were chosen for comparisons in this analysis. All test beam runs listed in table 1 were simulated with 100,000 π^- events, the noise being added to the digitised samples from the corresponding runs. Afterwards, the same selection procedure was applied

as to the data samples. The resulting number of pion events and the percentage of selected events are given in table 1.

3.2 Run and Event Selection

The data and simulation samples are selected from π^- runs in the range of 10 to 80 GeV. The run list and event selection follows the published software compensation analysis [3] and is summarised in table 1. The only deviation consists in the shower start, that was shifted from the first 5 layers to the 2nd to 6th layer in the HCAL in order to clean the data set from showers started in the last ECAL layer and/or in the gap between ECAL and HCAL. The events of runs with the same beam energy are merged and undergo the same requirements for the π^- event selection.
The data sample is reconstructed with the newest calice_soft version v04-08.
After the pre-selection of π^- events using the Cherenkov counter, to ensure the separation of electrons, and the reduction of noise by applying a threshold of 0.5 MIP on every cell, we reject

- muon and punch-through pion events by requiring more than 150 MIP deposited in the AHCAL.
- multi-particle events by requiring less than 80 MIP and 13 hits in the first 5 layers of the AHCAL.
- empty events by requiring more than 25 hits in the ECAL and 50 hits in the AHCAL.

To minimise leakage into the TCMT and fluctuations of the energy deposition in the ECAL, we select π^- events to

- start showering in the 2-6th HCAL layer by the ShowerStartClusterProcessor, details can be found in [12].
- be consistent with a particle passing the ECAL without hard interaction by requiring less than 50 hits.

The selected pion showers develop predominantly in the AHCAL while keeping the energy leakage into the TCMT as small as possible.

Figures 1 and 2 show the distributions of the visible energy and the number of hits in the AHCAL for data and MC for 10 and 80 GeV. The experimental data is

Table 1: List of data runs used in the analysis and sample statistics. The size of each simulated sample is 100,000 events per run.

run number	beam energy [GeV]	pre-selection data	selected pions in data		selected pions in MC (FTFP_BERT/QGSP_BERT)	
			N_{events}	in %	N_{events}	in %
330332, 330643, 330777, 330850	10	587,793	95,065	16.2	67,315/64,807	16.8/16.2
330328	15	140,441	24,044	17.1	16,963/ 16,245	17.0/ 16.3
330327	18	148,516	25,129	16.9	16,780/16,094	16.8/16.1
330649, 330771	20	379,270	61,538	16.5	32,902/31,979	16.5/16.0
330325, 330650	25	364,170	61,037	16.8	32,250/31,543	16.1/15.8
330551, 330960	35	404,309	57,981	14.3	31,626/31,460	15.8/15.7
330390, 330412, 330560	40	509,168	83,595	16.4	47,403/47,367	15.8/15.8
330550, 330559, 330961	45	520,600	84,583	16.3	47,263/46,836	15.8/15.6
330391, 330558	50	384,581	62,843	16.3	31,704/31,306	15.9/15.7
331556, 331568, 331655, 331664	60	787,208	133,618	17.0	62,666/62,302	15.7/15.6
330392, 330962, 331554, 331567, 331654	80	898,307	152,182	16.9	76,932/79,056	15.4/15.8

compared to the simulation, which shows some distinct differences. However, for all other energies the differences between data and MC are smaller. In all pre-selection plots for the energy sum distributions (see Figure 1a, 2a) and the number of hits (see Figure 1b, 2b) a peak around 100 MIP and 40 hits, respectively, are seen, much in excess compared to the simulation. This is due to the muon contamination in data, while in MC this peak arises only from punch-through pions. A second difference is a slight overestimation in the FTFP_BERT samples of the number of hits. The largest difference between data and MC is seen in Figure 2c, where both physics lists overestimate the AHCAL response. This trend was already seen and studied in [13].

3.2.1 AHCAL Simulation with $1 \times 1\,\mathrm{cm}^2$ Granularity

The original GEANT4 and MOKKA simulations of the test beam setup with the physics lists FTFP_BERT and QGSP_BERT have a granularity of $1 \times 1\,\mathrm{cm}^2$. Within the digitisation step, the energy depositions are merged into the desired cell size. Therefore to study the impact of the granularity, only the digitisation is repeated with a cell size of $1 \times 1\,\mathrm{cm}^2$, while the selected events stay the same. In the standard digitisation each cell is calibrated individually with the calibration constants extracted from the data runs. However, a $1 \times 1\,\mathrm{cm}^2$ AHCAL does not exist, and therefore average calibration constants are used to mimic the SiPM response. Another difference is the lack of dedicated noise runs, however for the new generation of SiPMs a strongly reduced noise rate is measured [14], thus the simulations are still realistic. The tile-to-tile crosstalk is kept at 15 %, even though the current design of scintillator tiles wrapped in reflective foil would eliminate this feature. A consequence of the reduced cell size is a decreased mean energy deposit per cell, which required an adjustment for the acceptance of a hit. The mean visible energy in MIP was compared to a series of different thresholds, and compared to the mean visible energy of the $3 \times 3\,\mathrm{cm}^2$ AHCAL with the 0.5 MIP threshold. The best agreement is seen for a 0.3 MIP threshold, which is a value realistically achievable, and applied in the following analysis.

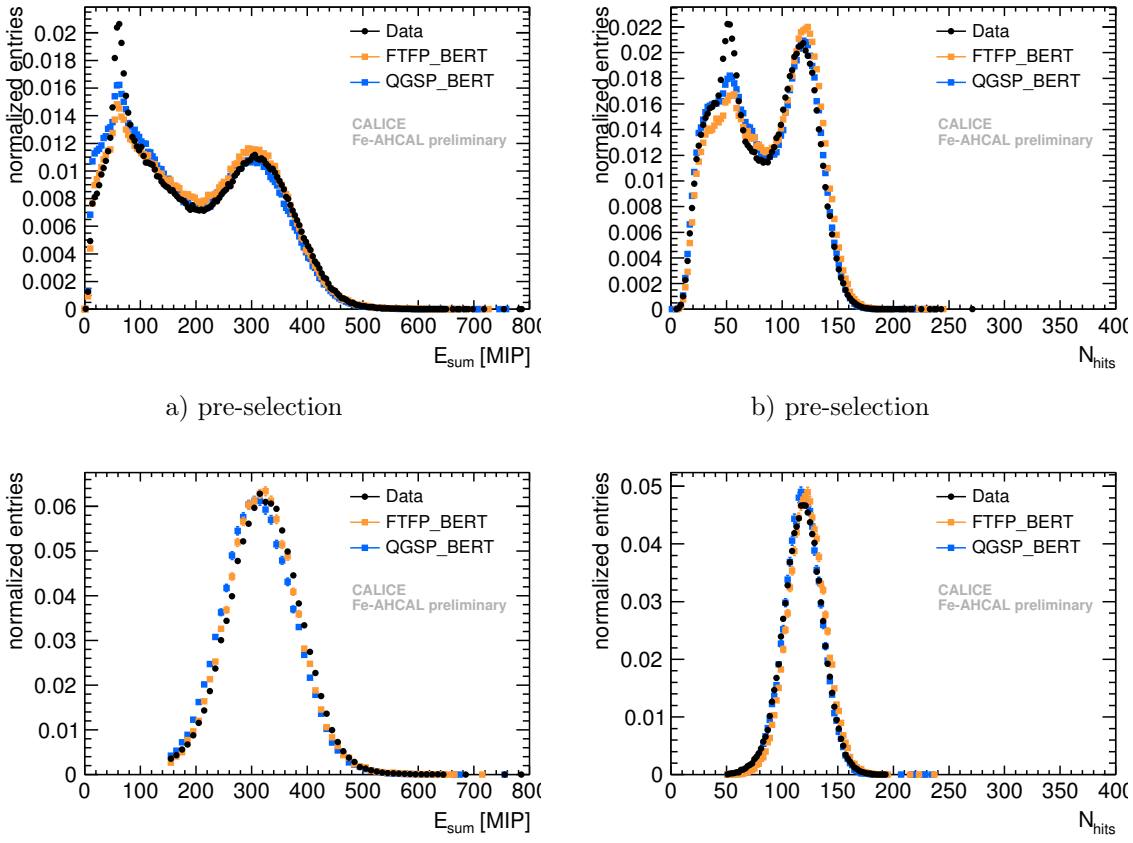

a) pre-selection

b) pre-selection

c) final selection

d) final selection

Figure 1: Distributions of the visible energy E_{sum} and the number of hits N_{hits} for $E_{beam} = 10\,GeV$, shown after the pre-selection in a) and b) and the final π^- selection in c) and d). The simulated FTFP_BERT data is shown in orange, the simulated QGSP_BERT data in blue, and the test beam data is represented by black points.

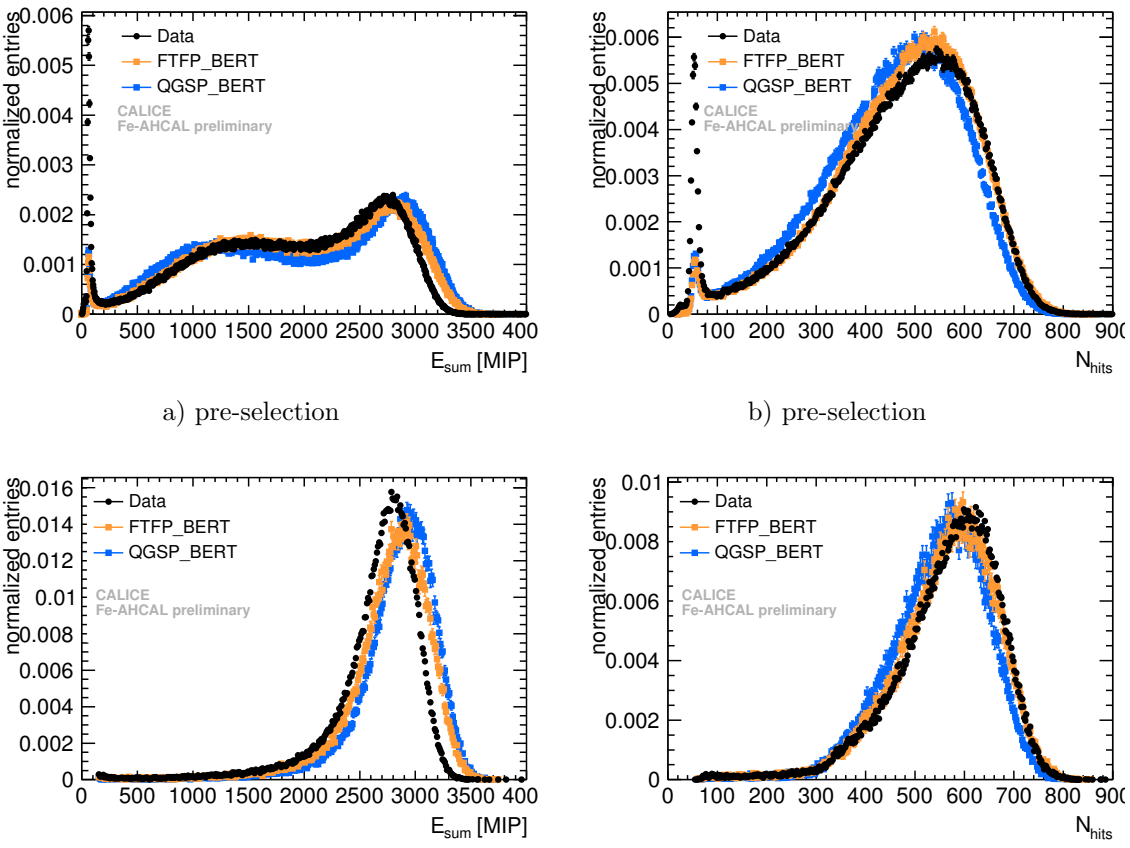

a) pre-selection

b) pre-selection

c) final selection

d) final selection

Figure 2: Distributions of the visible energy E_{sum} and the number of hits N_{hits} for $E_{beam} = 80\,GeV$, shown after the pre-selection in a) and b) and the final π^- selection in c) and d). The simulated FTFP_BERT data is shown in orange, the simulated QGSP_BERT data in blue, and the test beam data is represented by black points.

3.3 Systematic Uncertainties

The systematic uncertainties in data are estimated following [3] and [10], which both use the detailed analysis of the electromagnetic response [4]. The uncertainty of the beam energy ΔE_{beam} is taken into account with

$$\frac{\Delta E_{beam}}{E_{beam}} = \frac{12\%}{E_{beam}} \oplus 0.1\%. \tag{7}$$

The method to determine these values is described in [15].
The uncertainty on the reconstructed energy is dominated by the MIP to GeV conversion, which is estimated to be 0.9 %. The impact of the SiPM gain and saturation parameters are negligibly small [4].
The detector stability over time was tested by comparing the mean response in terms of the energy sum and the number of hits for all runs separately to the average mean response of all selected pion events. The deviations are found to be 0.9±0.1 % in $\langle E_{sum} \rangle$ and 1.4±0.2 % in $\langle N_{hits} \rangle$, see Figure 3.
In the following for the energies reconstructed from the energy sum the systematic uncertainty of the beam energy, the uncertainty from the MIP to GeV conversion, the uncertainty arising from the detector stability and the statistical errors are added in quadrature. For the energies reconstructed using the number of hits, the 0.9 % uncertainty from the MIP to GeV conversion is not taken into account.

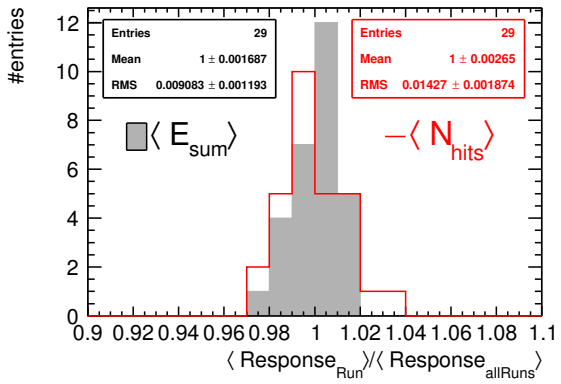

Figure 3: Detector stability in the observables E_{sum} and N_{hits} for pions with initial energies 10-80 GeV.

3.3.1 Systematics on Simulation

A systematic error on the simulations is estimated by generating two additional simulation samples with a minimum and maximum light leakage into the neighbouring cells. In the standard digitisation a light leakage of 15 % per tile is assumed, but other measurements showed values of 10 % and 18 % as well [4] [19]. These maximum deviations have been simulated and uncertainties on the mean energy sum (number of hits) of +2.2/-2.6 % (+3.4/-4.2 %) have been found.

4 Energy Reconstruction and Linearity

The goal of this analysis is a direct comparison of the reconstruction methods; analogue, digital, semi-digital and software compensation algorithms, applied to the same AHCAL data and a simulation of the AHCAL with a cell size of $1 \times 1\,\mathrm{cm}^2$. This includes using the same methods to extract the mean energy and the resolution. The distributions of the reconstructed energy from the number of hits are expected to show a non-Gaussian tail due to saturation effects. These tails are taken into account by using a Novosibirsk fit to describe the N_{hits}, E_{sum} and reconstructed energy E_{rec} distributions. The mean and width are extracted by the mean and RMS of a histogram filled following the Novosibirsk fit, details can be found in Chapter 4.4.1 of the previous CAN-049 version [20]. Earlier studies of the test beam data used the entire setup for the energy reconstruction. The energy in the ECAL and the TCMT complemented the measurement of the HCAL [3]. The conversion factors can be found in Appendix A.

Here the goal is to study the details of the energy reconstruction in the HCAL. Therefore, to be independent from the reconstruction procedures used by the other subdetectors, the TCMT measurement is not used, while the ECAL measurement is only used for the event selection. A fixed value of $0.3232 \pm 0.0002(\mathrm{stat.}) \pm 0.0322(\mathrm{syst.})$ GeV is taken as contribution of the track in the ECAL to the total shower energy (see appendix A). In the following the results of the different energy reconstruction schemes are shown for the two granularities next to each other; on the left the $3 \times 3\,\mathrm{cm}^2$ AHCAL data and MC comparison and on the right the results from the $1 \times 1\,\mathrm{cm}^2$ AHCAL simulations. In general the parameters needed for the energy reconstructions are extracted for the $3 \times 3\,\mathrm{cm}^2$ AHCAL from the test beam data and used also for the simulated data samples. For the $1 \times 1\,\mathrm{cm}^2$ AHCAL the parameters are extracted

from the FTFP_BERT simulation, since this is the physics list that describes the data best. They are used also for the QGSP_BERT samples.

4.1 Analogue

The analogue reconstructed energy for the $3 \times 3\,\mathrm{cm}^2$ Fe-AHCAL data and MC is given by

$$\mathrm{E_{rec,analogue}} = 0.3232\,\mathrm{GeV} + \frac{\mathrm{e}}{\pi} \cdot \omega \cdot \mathrm{E_{sum}} \cdot \mathrm{c}, \tag{8}$$

with the energy contribution of 0.3232 GeV from the track in the ECAL and otherwise the same variables as in Equation 2. To determine the energy reconstruction parameters for the $1 \times 1\,\mathrm{cm}^2$ AHCAL simulation samples the mean energy sum of the FTFP_BERT physics list is fitted, using

$$\langle \mathrm{E_{sum}} \rangle = \frac{(\mathrm{E_{beam}} - 0.3232\,\mathrm{GeV} - \mathrm{n_{1\times1}})}{\frac{\mathrm{e}}{\pi} \cdot \omega \cdot \mathrm{c_{1\times1}}}, \tag{9}$$

thus, assuming $\mathrm{E_{beam}} = \mathrm{E_{rec,analogue1\times1}}$, the energy can be reconstructed as

$$\mathrm{E_{rec,analogue1x1}} = 0.3232\,\mathrm{GeV} + \mathrm{n_{1\times1}} + \mathrm{E_{sum}} \cdot \frac{\mathrm{e}}{\pi} \cdot \omega \cdot \mathrm{c_{1\times1}}, \tag{10}$$

allowing a scaling by $\mathrm{c_{1\times1}}$ and an offset by $\mathrm{n_{1\times1}}$. The analogue response is sensitive to two effects: First the applied threshold, which introduces a minimum hit energy and in this way introduces a negative offset for the linear response (less than 0 MIP for a beam energy equal 0). Second the noise, that increases the response and generates a positive offset of the response (more than 0 MIP for a beam energy equal 0). Equation 9 allows an offset $\mathrm{n_{1\times1}}$ and a scaling of the response $\mathrm{c_{1\times1}}$, which is needed to achieve a satisfactory linearity after reconstruction, see Figure 5b. The positive value of $\mathrm{n_{1x1}}$=0.98 GeV can be traced back to the threshold and the lack of noise in the $1 \times 1\,\mathrm{cm}^2$ AHCAL simulation. In the $3 \times 3\,\mathrm{cm}^2$ AHCAL on the other hand, both effects usually compensate each other. The scaling needed in the $1 \times 1\,\mathrm{cm}^2$ AHCAL is found to be one percent, $\mathrm{c_{1x1}}$=1.01.

The comparison of the analogue reconstructed energy distributions between data and simulation of $3 \times 3\,\mathrm{cm}^2$ AHCAL is shown in Figure 4a. The mean reconstructed energy versus beam energy and the non-linearity is shown in Figure 5a. Similar to the observations in previous analyses, e.g. [10], the FTFP_BERT and the QGSP_BERT predictions lie slightly below the data at low energies and exceed the data by a few

percent at large beam energies. The $1 \times 1\,\mathrm{cm}^2$ AHCAL MC samples show the same trend between FTFP_BERT and QGSP_BERT, see Figures 4b and 5b.

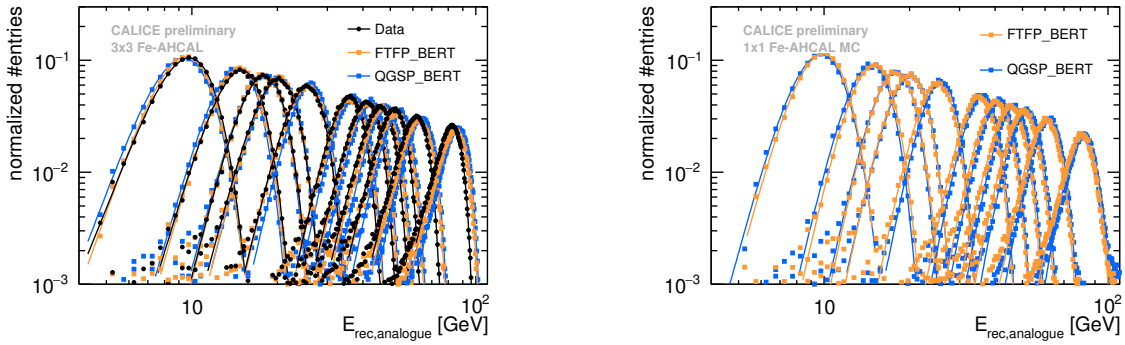

a) 3×3 b) 1×1

Figure 4: Analogue reconstructed energy distributions for the beam energies from 10 to 80 GeV; The black dots show the test beam data, the orange squares show the FTFP_BERT and the blue squares the QGSP_BERT simulated $E_{rec,analogue}$ distributions. The corresponding Novosibirsk fits are represented by solid lines.

4.2 Digital

The digital response is reconstructed from the number of hits above threshold. For the $3 \times 3\,\mathrm{cm}^2$ AHCAL the threshold value of 0.5 MIP is usually taken for AHCAL analyses ensuring a minimum contribution of noise to the reconstructed energy. This value is not optimal for the $1 \times 1\,\mathrm{cm}^2$ case. A threshold of 0.3 MIP in the $1 \times 1\,\mathrm{cm}^2$ AHCAL simulation is chosen to mimic the mean analogue response of the $3 \times 3\,\mathrm{cm}^2$ AHCAL. The mean digital responses before the correction for non-linearity are shown in Figures 6a and 6b and fitted with a power law $\langle N_{hits} \rangle = a \cdot (E_{beam} - m)^b$. The corresponding fit parameters are given in the caption. Both the data and the fit show a clear saturation behaviour. This is expected for the AHCAL granularity of (at best) $3 \times 3\,\mathrm{cm}^2$ cells, which is not well adapted to the digital reconstruction method, where several particles traversing a cell contribute the same amount to the reconstructed energy as a single particle. In the $1 \times 1\,\mathrm{cm}^2$ AHCAL simulation however, the saturation is reduced but still visible. The tails to smaller number of hits could be a hint that the cell size of $1 \times 1\,\mathrm{cm}^2$ is still not small enough to prevent saturation.
In the bottom part of the figures, the relative deviation of the $\langle N_{hits} \rangle$ from the fit function is shown. For the $3 \times 3\,\mathrm{cm}^2$ AHCAL data and simulation, the point at 20 GeV

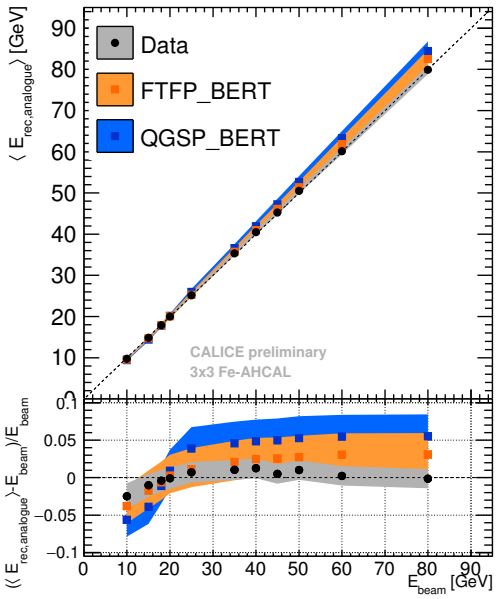

a) 3×3

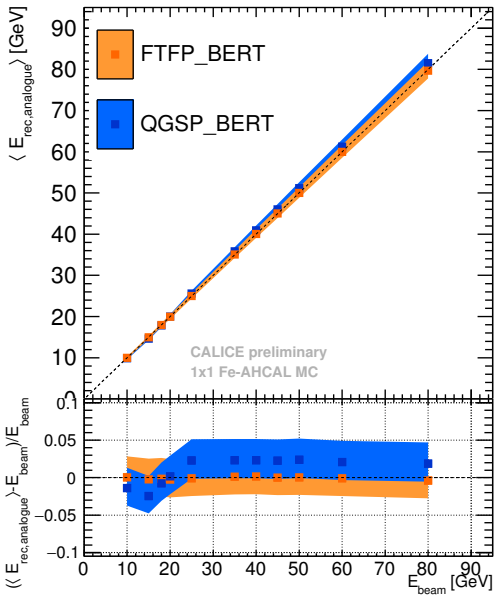

b) 1×1

Figure 5: Mean analogue reconstructed energy for pion showers versus beam energy; The test beam data is represented by black dots, the simulations using the FTFP_BERT and QGSP_BERT physics list in orange and blue squares, respectively. The bottom plots show the residuals to the beam energy with the bands indicating the systematic and statistical uncertainties. The purely statistical errors are smaller than the markers.

presents the strongest deviation from the fit curve, while the $1 \times 1\,\mathrm{cm}^2$ AHCAL simulations agree within their errors. The non-linearity introduced by the saturation is corrected on an event-by-event basis by assuming $\mathrm{E_{rec,digital}} = \mathrm{E_{beam}}$ and inverting the fit functions, leading to

$$\mathrm{E_{rec,digital}} = \mathrm{m} + \sqrt[\mathrm{b}]{\frac{\mathrm{N_{hits}}}{\mathrm{a}}}. \tag{11}$$

where the value of parameter m is fixed to 0.3232 GeV for the $3 \times 3\,\mathrm{cm}^2$ AHCAL and $\mathrm{m_{1x1}} = 3.0 \pm 1.2\,\mathrm{GeV}$ determined by the fit for the $1 \times 1\,\mathrm{cm}^2$ AHCAL simulation. The parameters a and b are extracted from the fit and given in the caption of Figure 6. In the following, the parameters determined from the fit to the data are used to reconstruct the energy of the real and also for the simulated data of the $3 \times 3\,\mathrm{cm}^2$ AHCAL. In the case of the $1 \times 1\,\mathrm{cm}^2$ AHCAL simulation, the values are taken from the FTFP_BERT simulation.

The resulting $\mathrm{E_{rec,digital}}$ distributions for data and simulation are compared in Figure 7a and 7b. The Novosibirsk fit functions used to extract the mean and the width of the $\mathrm{E_{rec,digital}}$ distribution are also shown. After the correction of the saturation behaviour, the data show agreement with a linear behaviour within $\pm 4\,\%$ (Figure 8a). Since the simulations are corrected with the same parameters as the data, they show slightly larger deviations from linearity than the data, with the largest deviation for QGSP_BERT of $\sim 8\,\%$ at 80 GeV. For the $1 \times 1\,\mathrm{cm}^2$ AHCAL simulation, see Figure 8b, the non-linearities are below 5 % for both physics lists.

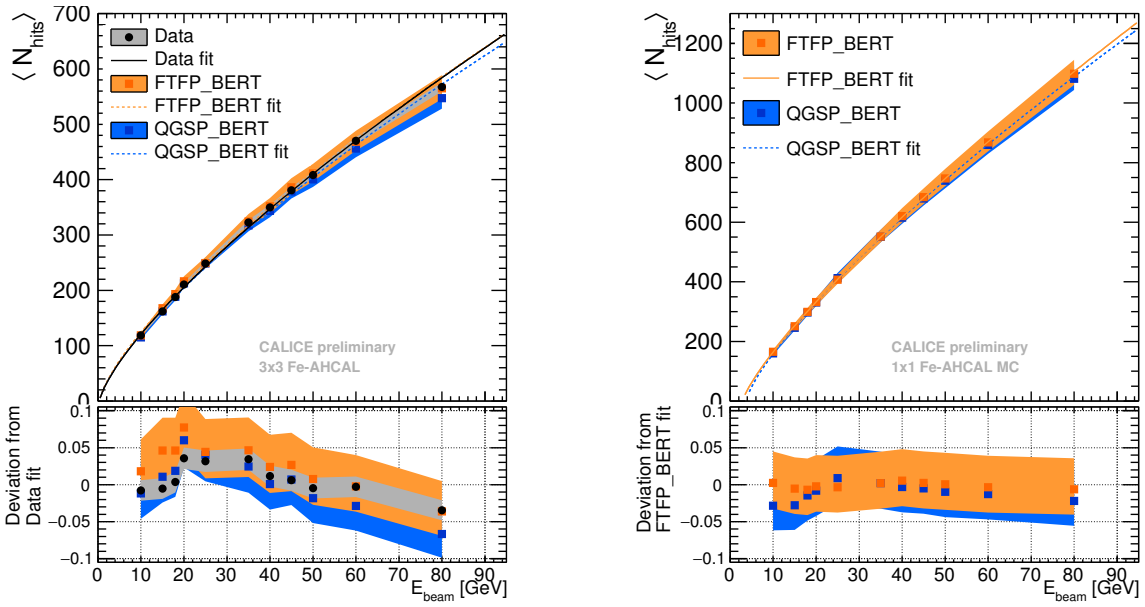

a) 3×3 b) 1×1

Figure 6: Mean digital response before the correction for non-linearity to pion showers, fitted with power law; $3 \times 3\,\mathrm{cm}^2$ AHCAL data: $a = 22.14 \pm 0.5\,\mathrm{GeV}^{-b}$, $b = 0.748 \pm 0.007$, $1 \times 1\,\mathrm{cm}^2$ AHCAL FTFP_BERT: $a = 34.7 \pm 7.5\,\mathrm{GeV}^{-b}$, $b = 0.80 \pm 0.05$. The plots on the bottom show the deviation from the power law fit. The bands indicate the statistical and systematic uncertainty added in quadrature, the statistical error only is smaller than the markers.

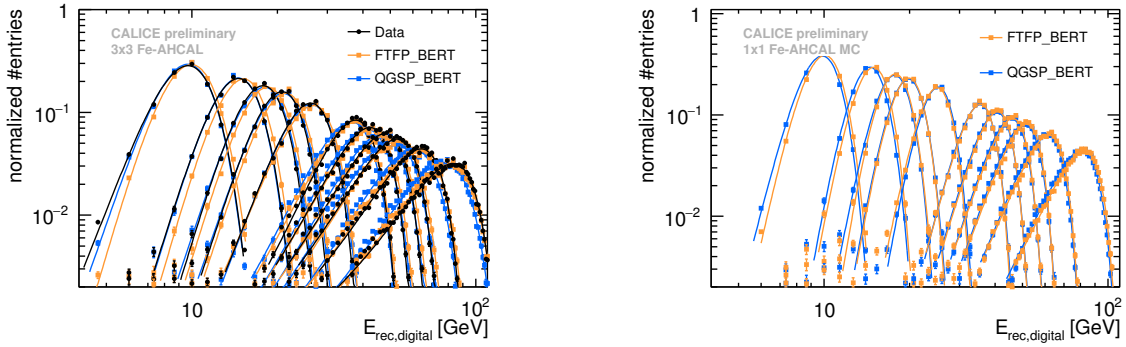

a) 3×3 b) 1×1

Figure 7: Digital reconstructed energy distributions for beam energies from 10 to 80 GeV; The black dots show the test beam data, the orange squares show the FTFP_BERT and the blue squares the QGSP_BERT simulated $E_{rec,digital}$ distributions. The corresponding Novosibirsk fits are represented by solid lines.

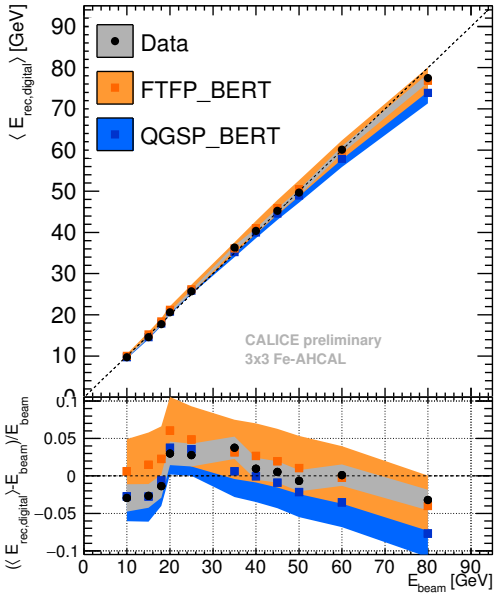

a) 3×3

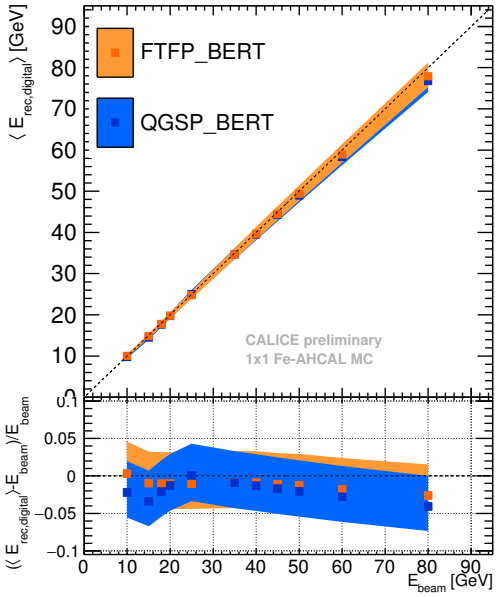

b) 1×1

Figure 8: Mean digital reconstructed energy for pion showers; The test beam data is represented by black dots, the simulations using the FTFP_BERT and QGSP_BERT physics list in orange and blue squares, respectively. The bottom plots show the residuals to the beam energy with the bands indicating the systematic and statistical uncertainties. The purely statistical errors are smaller than the markers.

4.3 Semi-Digital

The semi-digital energy reconstruction is done using Equation 4, where N_1 is the number of hits above the first threshold t_1 and below the second t_2, N_2 is the number of hits above the second t_2 below the third threshold t_3 and N_3 is the number of hits above t_3. For the determination of the calibration weights α, β and γ, 20,000 events are taken from each energy data set. These events have to have a total energy sum within the RMS90 of all E_{sum} to extract best possible weights for the majority of events. The χ^2-like function given in Equation 5 is minimised by ROOT using TMinuit2. The resulting weights are shown in Figure 10. The energy dependence of the weights is observed to be qualitatively the same for both granularities.
The lowest threshold is kept as used for all the other reconstruction schemes, while the higher thresholds have been optimised for both cell granularities by a scan of the χ^2 values, which give an estimate of the reconstruction accuracy, in the t_2-t_3 plain. The thresholds considered lay between 3 to 28 MIP and 5 to 105 MIP for t_2 and t_3, respectively. The optimal threshold values are summarised in Table 2. The threshold values optimised for the Micro-MEsh Gaseous Structure (Micromegas) SDHCAL prototype [17] are shown for comparison. The semi-digital response in terms of N_1, N_2 and N_3 is shown in Figure 9 and reveals a disagreement between data and MC in the number of very high energy hits N_3. This observation of 1.5 times higher number of high energy hits in simulation for high beam energies is consistent with the observed analogue hit energy spectra, that are further discussed in Chapter 4.4.

Table 2: The optimised thresholds used for the semi-digital reconstruction for both cell sizes and the SDHCAL prototype with Micromegas.

	t_1	t_2	t_3
$3 \times 3\,\mathrm{cm}^2$ Sci-Fe AHCAL	0.5	10.5	57
$1 \times 1\,\mathrm{cm}^2$ Sci-Fe AHCAL	0.3	10.5	30
$1 \times 1\,\mathrm{cm}^2$ Micromegas SDHCAL [17]	0.5	5	15

The semi-digital energy reconstruction of the $3 \times 3\,\mathrm{cm}^2$ AHCAL as well as the $1 \times 1\,\mathrm{cm}^2$ AHCAL data leads to much smaller tails towards low energies compared to the digital energy reconstruction. In Figure 11a and 11b the distributions of the semi-digital reconstructed energy for the test beam data and simulated FTFP_BERT and QGSP_BERT events are shown and a good agreement is observed for all energies.

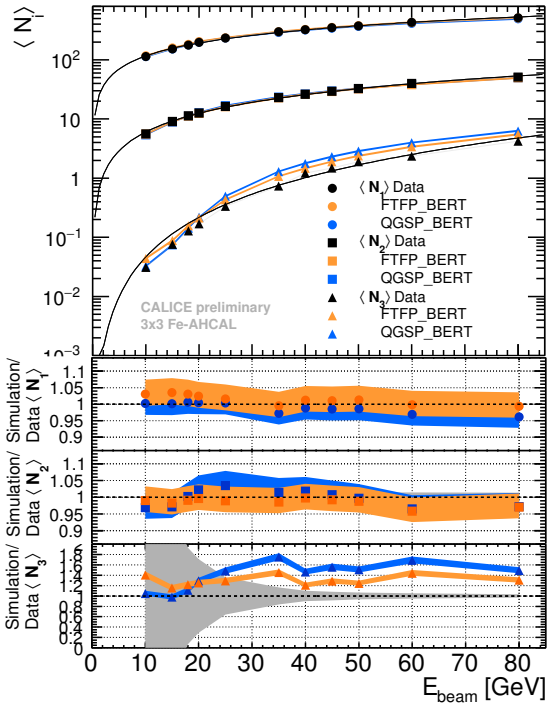

Figure 9: Mean semi-digital response of the $3 \times 3\,\mathrm{cm}^2$ AHCAL to pion showers; The test beam data (black markers), FTFP_BERT (orange markers) and QGSP_BERT (blue markers) for hits above the first, below the second threshold N_1, hits above the second, below the third threshold N_2 and hits passing the third threshold N_3. The lines represent fits with a power law and the bands the statistical and systematic uncertainty added in quadrature.

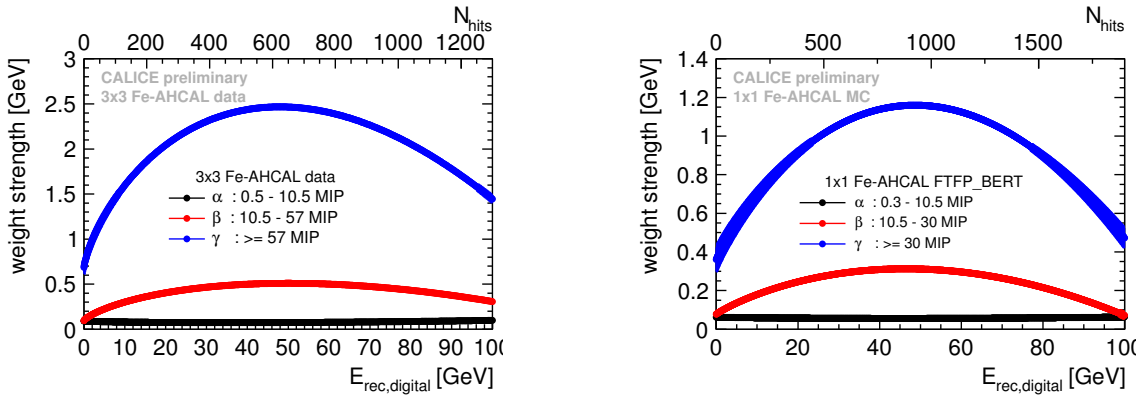

Figure 10: The weights for the semi-digital energy reconstruction are shown as a function of the total number of hits N_{hits} and the digitally reconstruction energy $E_{\mathrm{rec,digital}}$, which is calculated from N_{hits} by using Equation 11. The width of the curves correspond to the statistical errors, correlations are taken into account.

The non-linearities are always smaller than ±10 % for all energies, see the bottom plots of Figures 12a and 12b.

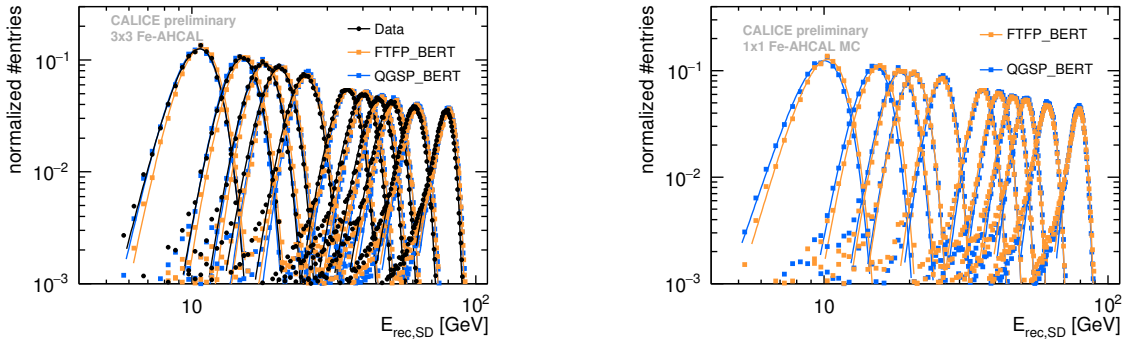

a) 3×3 b) 1×1

Figure 11: Semi-digital reconstructed energy distributions for beam energies from 10 to 80 GeV; The black dots show the test beam data, the orange squares show the FTFP_BERT and the blue squares the QGSP_BERT simulated $E_{rec,SD}$ distributions. The corresponding Novosibirsk fits are represented by solid lines.

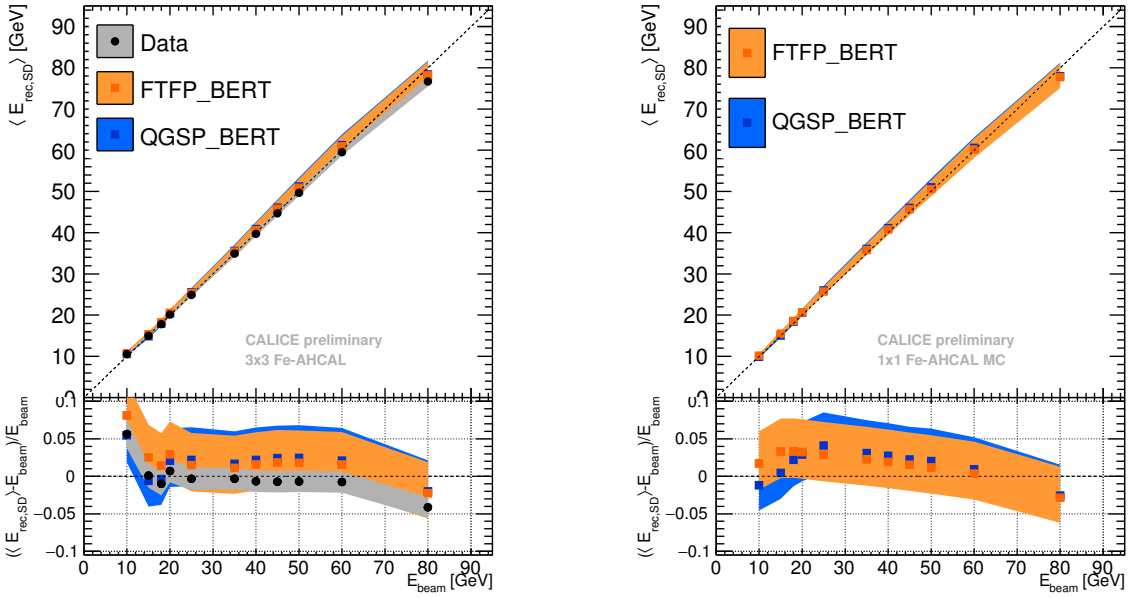

a) 3×3 b) 1×1

Figure 12: Mean semi-digital reconstructed energy for pion showers; The test beam data is represented by black dots, the simulations using the FTFP_BERT and QGSP_BERT physics list in orange and blue squares, respectively. The bottom plots show the residuals to the beam energy with the bands indicating the systematic and statistical uncertainties. The purely statistical errors are smaller than the markers.

4.4 Analogue Software Compensation

The energy reconstruction with the new software compensation algorithm is done following Equation 6, where the applied weights are dependent on the individual hit energies E_i and the total energy via the visible energy E_{sum}. For practical reasons, the number of hit energy ranges with constant hit energy weights is in this analysis limited to 8, which still requires the determination of 8×3 (each weight is described as a 2nd order polynomial of E_{sum}) $= 24$ parameters in the χ^2 minimisation, following Equation 5. This non-optimised classification of the hits is visualised by shadowed areas in the hit energy spectra, see Figures 13a and 13b. The comparison between data and simulations reveals a nice agreement, always better than 10 % for beam energies below 30 GeV. For higher beam energies the simulations overestimate the number of hits with very high energy >60 MIP. The differences between the physics lists are smaller than 5 %.
The energy range is affected by the lowered threshold from 0.5 to 0.3 MIP, going from 3×3 to $1 \times 1\,\mathrm{cm}^2$, and the significantly smaller hit energy densities in the $1 \times 1\,\mathrm{cm}^2$ cells. Therefore the hit energy ranges of the weights are adapted to the granularity.

The weights used for the energy reconstruction in the $3 \times 3\,\mathrm{cm}^2$ AHCAL are determined from data and applied to all the samples. In the $1 \times 1\,\mathrm{cm}^2$ AHCAL case, the weights are determined from the FTFP_BERT physics list and applied to both simulation samples. The weights are shown and further discussed in Chapter 6.2. The reconstructed energy distributions, shown together with the Novosibirsk fits in Figure 14a and 14b, exhibit narrow peaks. The fit range needed to be limited to $\mu \pm 2.5\sigma$ in order to achieve a satisfying χ^2. In the distributions small tails to the left hand side are seen, which is expected due to the limited number of layers (energy leakage into the TCMT). In Figure 15a the linearity is shown, and a nice agreement between data and simulation, especially with the FTFP_BERT physics list is seen. Thus the earlier discussed difference in the number of high energy hits does not have a huge impact on the overall energy reconstruction. In the higher granularity case, the non-linearities for both physics lists do not exceed 5 %, see Figure 15b. Except for the two lowest beam energies, the physics lists show a nearly identical behaviour.

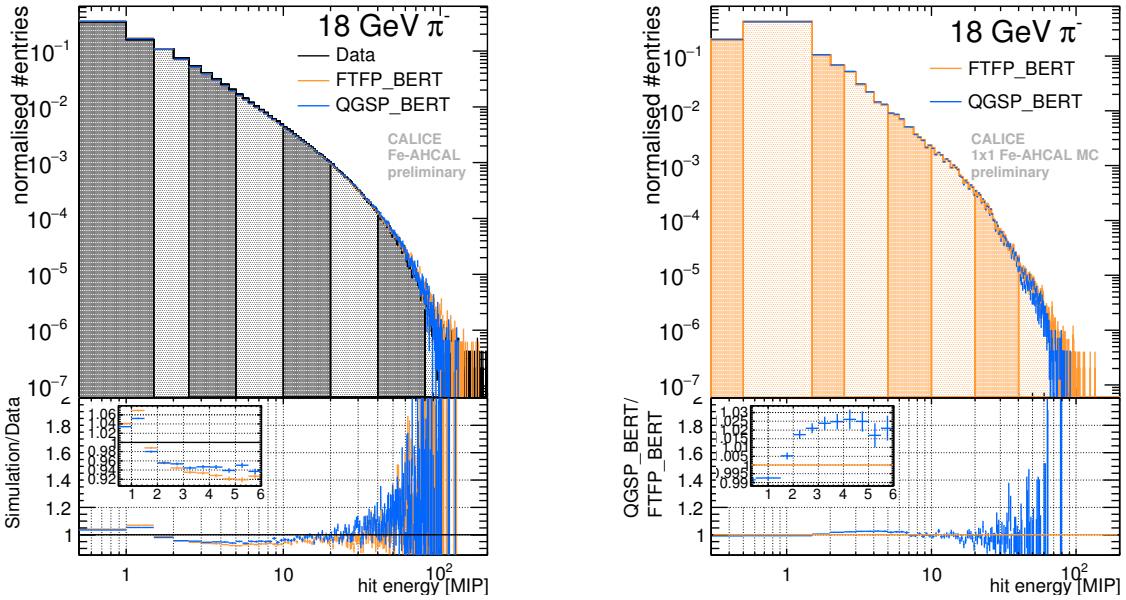

a) 3×3 b) 1×1

Figure 13: The hit energy spectra for 18 GeV π^- showers in the 3×3 and $1 \times 1\,\mathrm{cm}^2$ AHCAL, the test beam data shown in black, compared to simulated FTFP_BERT and QGSP_BERT data samples in orange and blue. At the bottom parts the deviation between data and simulation, and between FTFP_BERT and QGSP_BERT simulations are shown respectively. The errors shown are purely statistical.

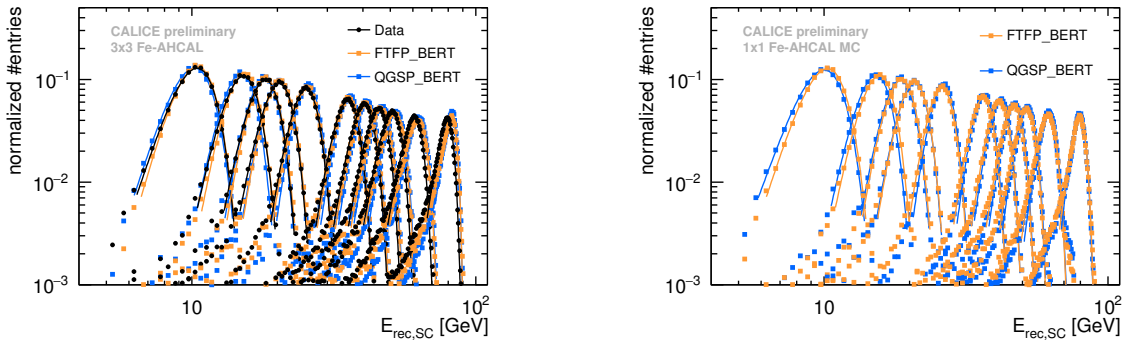

a) 3×3 b) 1×1

Figure 14: Reconstructed energy distributions for the beam energies from 10 to 80 GeV after applying the software compensation algorithm; The black dots show the test beam data, the orange squares show the FTFP_BERT and the blue squares the QGSP_BERT simulated $E_{rec,SC}$ distributions. The corresponding Novosibirsk fits are represented by solid lines.

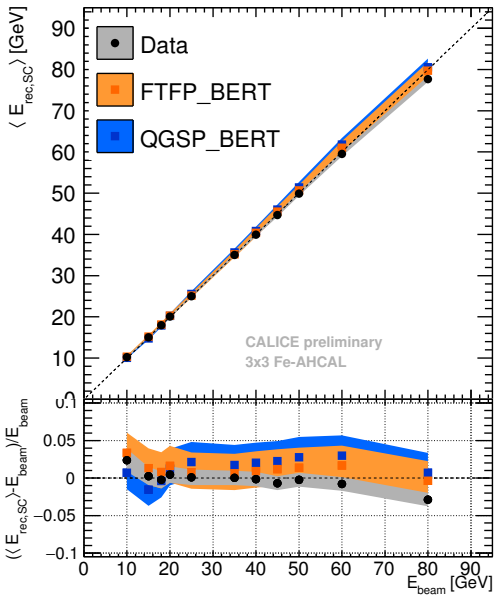

a) 3×3

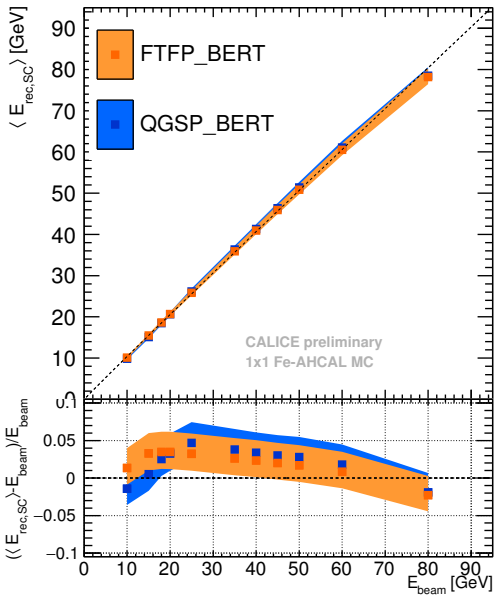

b) 1×1

Figure 15: Mean reconstructed energy for pion showers after applying the software compensation algorithm; The test beam data is represented by black dots, the simulations using the FTFP_BERT and QGSP_BERT physics list in orange and blue squares, respectively. The bottom plots show the residuals to the beam energy with the bands indicating the systematic and statistical uncertainties. The purely statistical errors are smaller than the markers.

5 Energy Resolution

All four reconstruction methods show a reasonable linearity, which guarantees a correct energy reconstruction in all cases. Therefore the resolutions can be compared. The impact of the AHCAL granularity on the digital or semi-digital reconstruction methods and on the resolution is expected to be strong for the highest beam energies. The functional form usually employed to fit the relative energy resolution, which consists of a stochastic, a constant and a noise term, does not accommodate for a degrading resolution at higher energies. Therefore, we introduce a fourth term with variable exponent for the energy dependence, similar to the approach used in [18]:

$$\frac{\sigma_{\mathrm{rec}}}{\langle \mathrm{E_{rec}} \rangle} = \frac{\mathrm{a}}{\sqrt{\mathrm{E_{beam}[GeV]}}} \oplus \mathrm{b} \oplus \frac{\mathrm{c}}{\mathrm{E_{beam}[GeV]}} \oplus \mathrm{d} \left(\frac{\mathrm{E_{beam}[GeV]}}{100} \right)^{\mathrm{e}}. \qquad (12)$$

The fourth term can account for leakage as well as saturation effects. For each reconstruction method only the parameters needed for a reasonable description of the data are left free. A direct comparison of the extracted values between the different methods is therefore difficult, and the fits should mainly guide the eye.

5.1 Analogue

The relative resolution for the analogue energy reconstruction of the AHCAL pion data and of the corresponding FTFP_BERT and QGSP_BERT simulations are shown in Figure 16a as a function of the beam energy. The FTFP_BERT simulation describes the data quite well for energies below 50 GeV. For higher energies the resolution of the simulated data lies about 5 % above the data. The QGSP_BERT simulation achieves a resolution of up to 5 % better for energies higher than 20 GeV. Test beam data and simulation show a decreasing relative resolution with increasing energy, as expected if leakage or saturation play only a minor role. Therefore, the resolutions can be parametrised without the fourth term in Equation 12.
In Figure 16b the relative resolution of the analogue energy reconstruction of the AHCAL in $1 \times 1\,\mathrm{cm}^2$ granularity is shown for the two physics lists. Since the FTFP_BERT simulation shows the best agreement with data, these points are the only ones fitted. In comparison with the resolution of the $3 \times 3\,\mathrm{cm}^2$ AHCAL data, the resolution improves up to one percent in absolute values for lower energies and reaches approximately the same values for higher beam energies. These small deviations are possibly

due to two differences: the lack of noise in the 1×1 simulations and the different threshold settings.

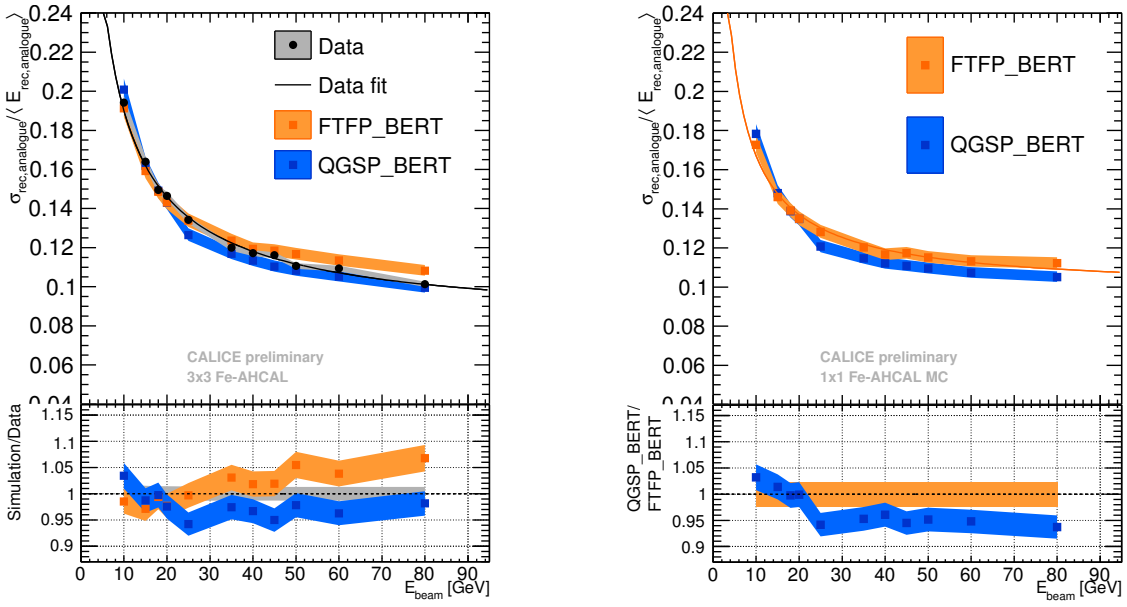

a) 3×3 b) 1×1

Figure 16: Analogue energy resolution for test beam data, FTFP_BERT and QGSP_BERT simulated events, fitted with Equation 12. At the bottom the deviations between the test beam data and simulations, between the FTFP_BERT and QGSP_BERT physics lists are shown, respectively.

5.2 Digital

In Figure 17a and 17b, the relative energy resolutions of the digital reconstruction method applied to AHCAL pion data, FTFP_BERT and QGSP_BERT simulations are compared. Both data and simulation of the $3 \times 3\,\mathrm{cm}^2$ AHCAL show a strong worsening of the resolution towards large energies, and a minimum resolution of about 16 % for energies around 20 GeV. Data and simulation agree very well within the errors. The strong rise at larger energies can be fitted when taking into account the fourth term in Equation 12. Since the lowest beam energy used in this analysis is 10 GeV, the terms decreasing with increasing energy in Equation 12 are not well constrained. For this reason the values for a and b are fixed to zero in the fit to data and simulation.

The finer granularity strongly improves the resolution over the full energy range. However, the behaviour of a degradation from a certain energy onwards stays the same. The minimum is seen around 25 GeV and reaches about 11 %. Not only the minimum is shifted, but the increase after 25 GeV is less steep than for the larger granularity. Both physics lists agree very well within their errors.

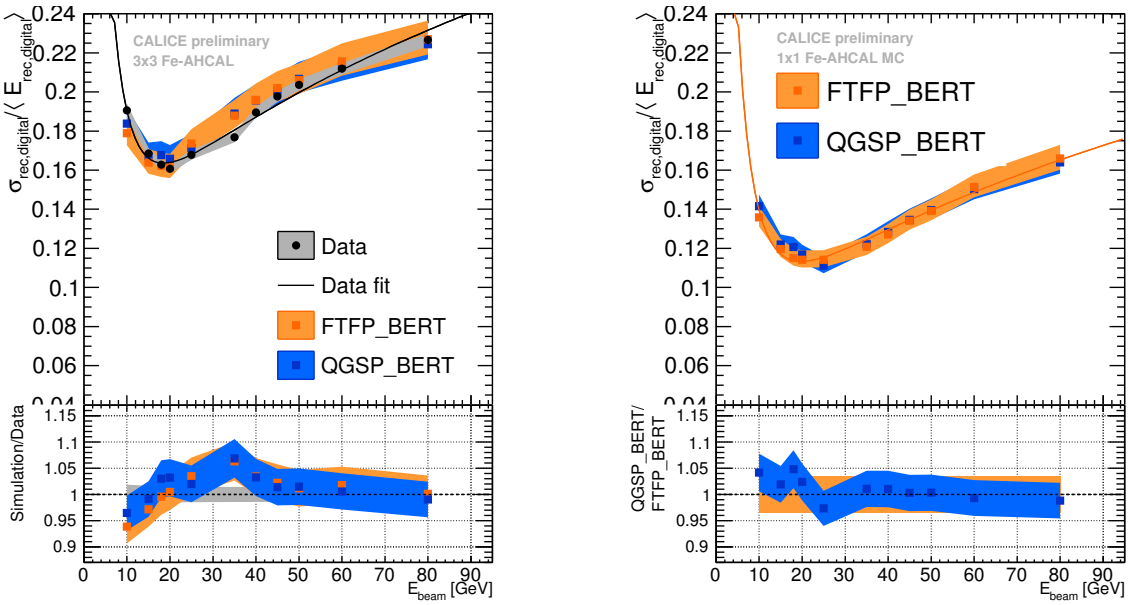

a) 3×3 b) 1×1

Figure 17: Digital energy resolution for test beam data, FTFP_BERT and QGSP_BERT simulated events, fitted with Equation 12. At the bottom the deviations between the test beam data and simulations, between the FTFP_BERT and QGSP_BERT physics lists are shown, respectively.

5.3 Semi-Digital

The relative resolution of the semi-digital reconstruction method shows yet a different dependence on the beam energy, see Figure 18a and 18b. The weighting method, which is based on a χ^2 function, assumes σ_E to follow a $\sqrt{E_{beam}}$ behaviour. The resolution observed for the $3 \times 3\,cm^2$ AHCAL shows a linear decrease for energies above 20 GeV, down to 8 % at 80 GeV. This behaviour is not well described by Equation 12 and therefore the fit is not shown in Figure 18a. Overall the FTFP_BERT simulation agrees well with the data in the analysed energy range, while the QGSP_BERT simulation shows a 5-7 % better resolution in the linear region. The resolution of the simulated $1 \times 1\,cm^2$ AHCAL shows an improvement with increasing beam energy, also following a nearly linear behaviour for beam energies above 20 GeV, down to about 6 % at 80 GeV.

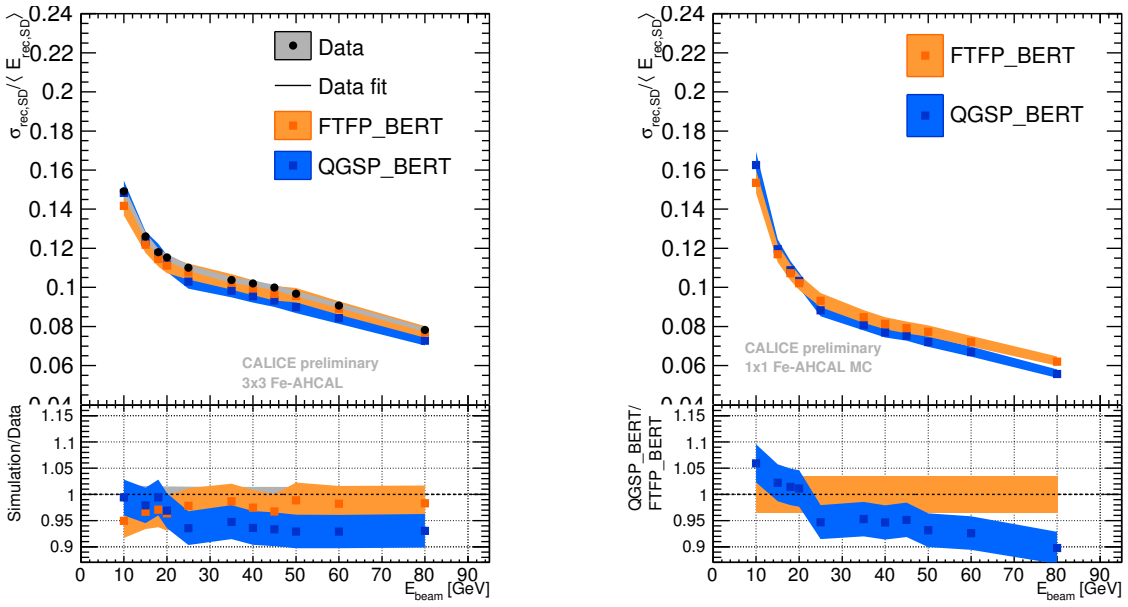

a) 3×3 b) 1×1

Figure 18: Semi-digital energy resolution for test beam data, FTFP_BERT and QGSP_BERT simulated events. At the bottom the deviations between the test beam data and simulations, between the FTFP_BERT and QGSP_BERT physics lists are shown, respectively.

5.4 Analogue Software Compensation

The relative resolution of the energy reconstructed with the software compensation technique is shown in Figure 19a and 19b. The comparison of the test beam data and simulation reveals the strongest deviations in the resolution for the QGSP_BERT physics list, which exceeds 10 % at 80 GeV. The FTFP_BERT simulation agrees with the data within 5 %. Generally, the resolutions decrease with increasing beam energy and the test beam data achieve a resolution of 6.5 % at 80 GeV. However, the behaviour can not be well described by Equation 12, therefore no fit is included in Figure 19a and 19b.

The impact of the software compensation algorithm on the resolution of the $1 \times 1\,\mathrm{cm}^2$ AHCAL is shown in Figure 19b. The resolution improves compared to the $3 \times 3\,\mathrm{cm}^2$ AHCAL up to 1 % in absolute values in the energy range of 30 to 80 GeV. The deviations between simulations with different physics lists are the largest for this reconstruction method, reaching up to ∼10 %. This difference originates from the differences in the hit energy spectra, discussed in Chapter 4.4.

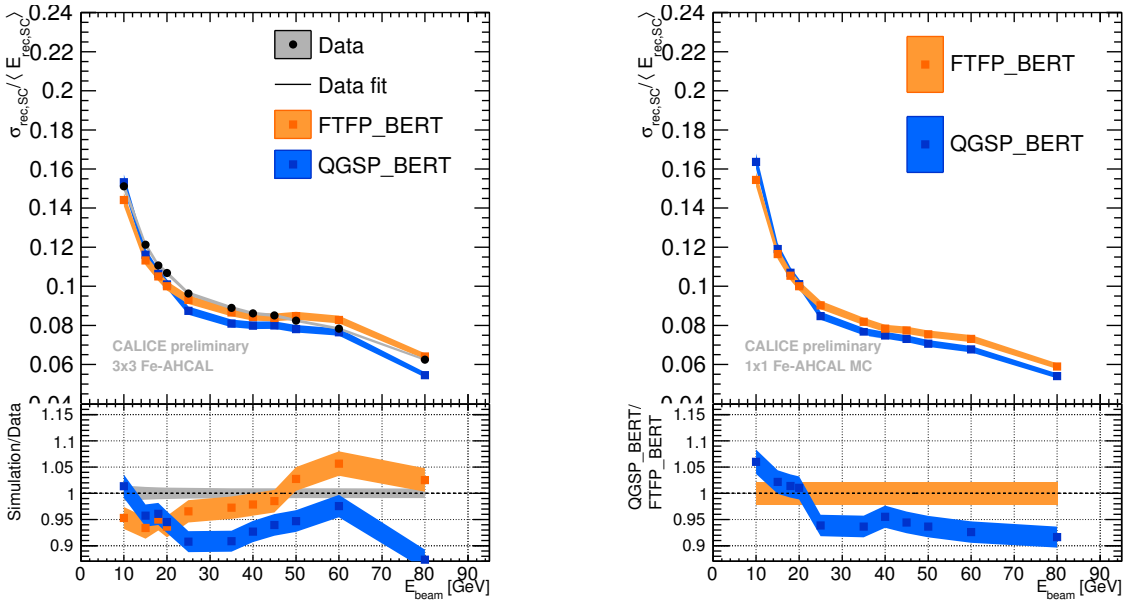

a) 3×3 b) 1×1

Figure 19: Energy resolution observed applying software compensation algorithms for the test beam data, FTFP_BERT and QGSP_BERT simulated events. At the bottom the deviations between the test beam data and simulations, between the FTFP_BERT and QGSP_BERT physics lists are shown, respectively.

6 Comparison of Energy Resolutions

6.1 Comparison between Reconstruction Procedures

The resolutions obtained with the different reconstruction methods are compared by applying them on the same data samples. The results obtained for AHCAL data and simulation samples are shown in Figure 20. A parametrisation of the best resolution obtained in a previous analysis [3] with AHCAL data, by applying software compensation techniques is also shown. In the comparison it is important to keep in mind that in the earlier analysis [3], the TCMT and the ECAL are included in the energy reconstruction. Here a simplified treatment of the ECAL is used and the TCMT contribution is neglected. The deviations from linearity of the methods studied in this analysis are also shown in the upper part of Figures 20a and 20b.
In case of the $3 \times 3\,\mathrm{cm}^2$ granularity at the lowest energy points, the analogue and digital reconstruction procedures show rather similar resolutions. For larger energies, the resolution of the analogue reconstruction method continues to decrease, while the digital resolution increases dramatically. The best resolution of all four methods for the whole energy range is found using the analogue software compensation algorithm. For energies up to 20 GeV it is indeed as good as the resolution reached with the software compensation techniques developed in the past. The difference observed at higher beam energies in Figure 20a is caused by energy leakage and is enhanced by the different extraction of the mean and width of the reconstructed energy distributions. This analysis takes tails due to saturation and energy leakage into account by using a Novosibirsk function, while the past analysis only considered the Gaussian peak in the range $\mu \pm 1.5\,\sigma$. The semi-digital reconstruction and the software compensation both apply weights to the energy depositions in a shower depending on the hit energy. The semi-digital reconstruction achieves a resolution similar to the software compensation for the lowest energy, 10 GeV. For higher beam energies the resolution follows a similar tendency as the software compensation but absolute values 1-2 % worse.
The AHCAL with reduced ($1 \times 1\,\mathrm{cm}^2$) cell size is expected to show an improved resolution for the (semi-)digital readout schemes, which is what is observed in Figure 20b. Compared to the classical analogue energy reconstruction the digital reconstruction shows better results for beam energies below 35 GeV. This improvement despite the reduction of information can be explained by the shape of the analogue cell signal,

which follows a Landau distribution that is characterised by a long tail to high values. By counting cells above a certain signal amplitude, the signal fluctuations to too high values are removed and thus the energy reconstruction is improved, especially for low beam energies with a high number of low energy hits. A degradation due to saturation effects of the digital resolution is only observed above 25 GeV. The increase of the number of thresholds from 1 to 3, digital to semi-digital, has a huge impact on the resolution in the $1 \times 1\,\mathrm{cm}^2$ AHCAL. This is different from the observation in the analysis of SDHCAL data, where the resolutions obtained with a digital and the semi-digital reconstruction method agree up to energies of about 40 GeV, and the semi-digital procedure improves the resolution only for larger energies [8].
The best resolution is achieved by applying either a weighting by the software compensation algorithm or by the semi-digital energy reconstruction. Which is expected because both methods apply energy dependent weights, which are determined by a χ^2 minimisation that optimises the resolution. For both methods a decreasing resolution with increasing beam energy is observed. The semi-digital resolution achieves at 80 GeV 6 %, while the software compensation shows a roughly 1 % better resolution in the energy range between 25 and 60 GeV. Otherwise the results are very similar.

6.2 Comparison between Semi-Digital and Software Compensation Weights

The weight determinations of the semi-digital energy reconstruction and of the software compensation algorithm is very similar. The biggest difference lies in the usage of the hit energy information. The semi-digital weights follow $\alpha_i\,[\mathrm{GeV}] = a_i + b_i \cdot N_{hits} + c_i \cdot N_{hits}^2$, thus using N_{hits} as an estimate of the beam energy, and are used for the reconstruction by

$$E_{rec,SD} = \sum_{i=1}^{3} \alpha_i\,(N_{hits}) \cdot N_i. \tag{13}$$

The software compensation weights follow $\omega_j \left[\frac{\mathrm{GeV}}{\mathrm{MIP}}\right] = a_j + b_j \cdot E_{sum} + c_j \cdot E_{sum}^2$ and are in this way determined using a beam energy estimate via E_{sum}. In the reconstruction

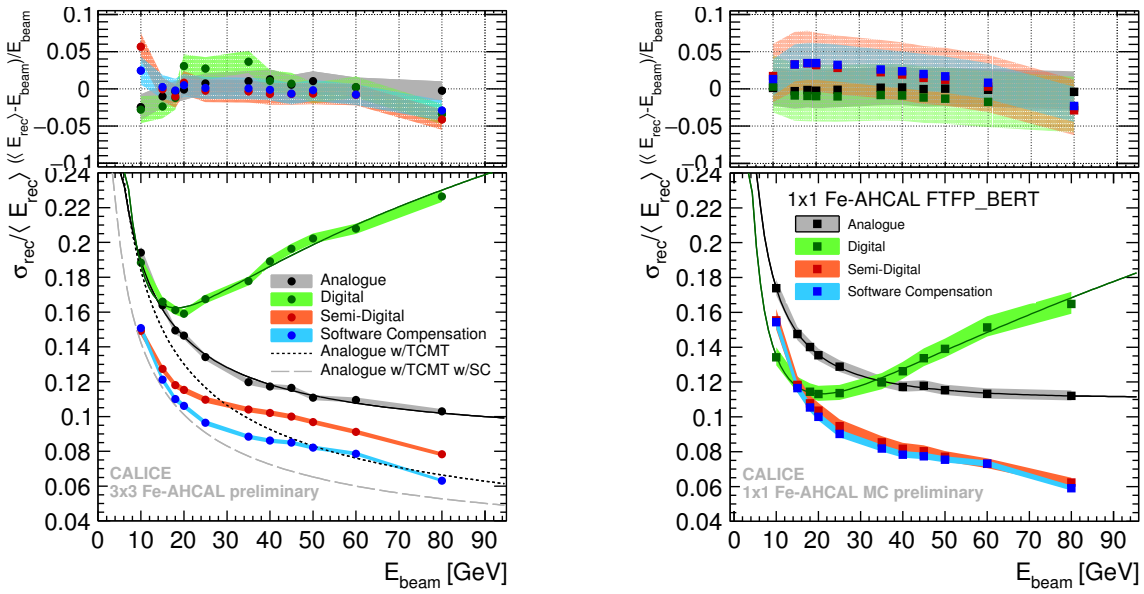

a) 3×3 b) 1×1

Figure 20: Energy dependence of the relative energy resolution of the AHCAL test beam data in (a) and the simulation with $1 \times 1\,\mathrm{cm}^2$ granularity and the FTFP_BERT physics list in (b), obtained using different approaches for the energy reconstruction of pions: analogue (black), digital (green), semi-digital (red) and applying the software compensation algorithm (blue). The dashed and dotted curves in (a) show the resolution achieved in [3] with and without software compensation techniques, using the energy deposits in the TCMT and in the ECAL in addition to the AHCAL. The plots on the top show the residuals to the beam energy with the bands indicating the systematic and statistical uncertainties. The purely statistical errors are smaller than the markers.

however, each hit energy e_j is taken into account, following Equation 6:

$$E_{rec,SC} = \sum_{j=0}^{N_{hits}} \omega\left(e_j, E_{sum}\right) \cdot e_j. \tag{14}$$

To show that the semi-digital weights α_i implicitly dependent on the individual hit energy, the three weights (for hits in the $t_1 - t_2$, $t_2 - t_3$, $> t_3$ range) are divided by the hit energy α_i/e_j and shown in Figure 21 as green lines for each beam energy. The software compensation and semi-digital weights show both a decrease with increasing hit energy. However the software compensation weights show an increase of the weight strength for the last two, high energy bins for high beam energies. The weights for the first and the last hit energy bin show a strong beam energy dependence. The differences between the software compensation and semi-digital weights are more pronounced for the $3 \times 3\,\mathrm{cm}^2$ AHCAL test beam data (Fig. 21a) than for the $1 \times 1\,\mathrm{cm}^2$ AHCAL simulation with the FTFP_BERT physics list (Fig. 21b). This could be an effect of the different cells sizes, that are not taken into account here.

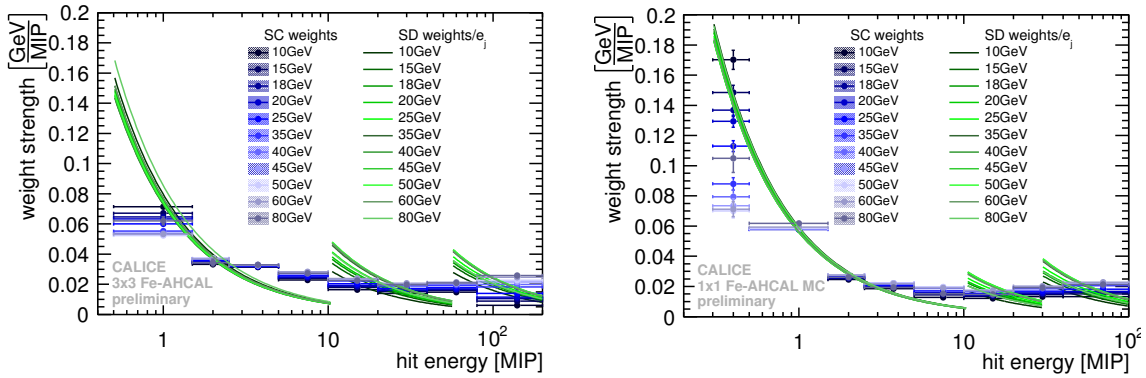

a) 3×3 b) 1×1

Figure 21: The weights used for the software compensation and semi-digital energy reconstruction in the 3×3 and $1 \times 1\,\mathrm{cm}^2$ AHCAL are shown as a function of the hit energy for the beam energies of 10-80 GeV. The software compensation weights are shown as blue bars covering a certain hit energy range, the semi-digital weights are shown as green lines following a $1/e_j$ behaviour.

Since the digital treatment of hits shows very good results for low beam energies (see Figure 20b), the software compensation algorithm is tested to some extent with counting hits of a certain energy range. Three options have been considered; The hits within the first two hit energy bins ($\sim$ 1 MIP) are counted and the weights

parametrised as 2nd order polynomials of the total number of hits (shown in Figure 22 as "SC + 2 digital bins"). The very high energy hits are counted and included in the energy reconstruction digitally (shown as "SC + truncation"). Additionally the software compensation algorithm is tested using the same classification of hits as the semi-digital reconstruction (shown as "SC with 3 thresholds").

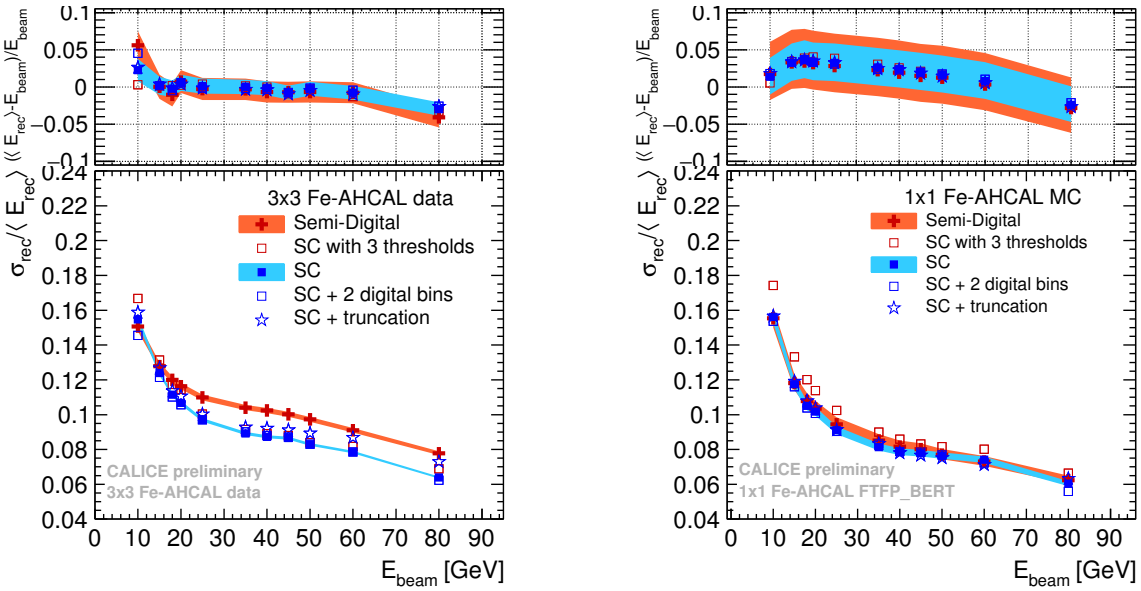

a) 3×3 b) 1×1

Figure 22: Energy dependence of the relative energy resolution of the AHCAL data and simulation with FTFP_BERT physics list, obtained using different weighting approaches for the energy reconstruction of pions: semi-digital (red cross), with software compensation techniques (blue squares) and variation of the software compensation algorithm (open markers). The plots on the top show the residuals to the beam energy with the bands indicating the systematic and statistical uncertainties. The purely statistical errors are smaller than the markers.

For both granularities no strong preference is observed for the different methods of hit treatments within the software compensation algorithm. The linearities achieved are shown in the plots on the top of Figure 22. It has to be mentioned that a positive/negative deviation from linearity improves/degrades the relative resolution artificially. However, all observed non-linearities are small enough that the results of the comparison between reconstruction methods of absolute and relative resolutions agree.

A slight improvement is seen in the resolution for 10 and 80 GeV by using two digital energy bins in the 1 MIP range (compare open and filled blue squares). The reso-

lution using the software compensation algorithm with only 3 instead of 8 weights degrades about 0.5 % to 1 % in absolute values. This is observed for both granularities (compare open red squares with filled blue squares). This is most probably an effect of the thresholds optimised for the semi-digital reconstruction and could be further improved by optimising the energy ranges for the software compensation algorithm. The weights for the different methods are shown for the $1 \times 1\,\mathrm{cm}^2$ AHCAL FTFP_BERT simulation in Appendix B.

6.3 Impact of the Granularity and Calorimeter Technology

The impact of the granularity on the reconstruction procedures is shown in terms of energy resolution for the digital and semi-digital energy reconstruction in Figure 23a and 23b. The results are also compared to the test beam data of the DHCAL [7] and SDHCAL [8] prototypes. For the digital reconstruction the resolution is improved between 4.5 and 6.5 % by reducing the granularity from 3×3 to $1 \times 1\,\mathrm{cm}^2$, improving more with increasing beam energy. The resolutions are compared to the full calibrated DHCAL data [7]. The comparison reveals that the digitally read out AHCAL shows a better resolution for the low beam energies <15 GeV even with a granularity of $3 \times 3\,\mathrm{cm}^2$. The increase in the resolution due to saturation happens much earlier and much stronger in the scintillator-steel (Sci-Fe) HCAL compared to the DHCAL data. But it has to be mentioned that the DHCAL analysis [7] uses a Gaussian fit to determine the resolution, which does not take tails due to saturation effects into account.

The improvement due to a finer granularity on the semi-digital resolutions is ∼2 % for beam energies larger than 25 GeV. For the lower beam energies the improvement is smaller and for 10 GeV there is basically no difference. Compared to the SDHCAL data points from [8], the AHCAL simulations in both granularities show a better resolution for beam energies smaller than 60 GeV. Between 60 to 80 GeV however the resolutions of the SDHCAL data and AHCAL simulation in $3 \times 3\,\mathrm{cm}^2$ agree. It has to be mentioned that the SDHCAL data was recorded with 48 active layers, while these simulations are done for only 38 AHCAL layers. However, the SDHCAL event selection is constrained to have the showers started after the first 5 layers to remove the electron contamination. In conclusion it has to be mentioned that the threshold settings of the SDHCAL prototype have not been optimised. Therefore the semi-digital resolution of the $1 \times 1\,\mathrm{cm}^2$ AHCAL is expected to show a better performance.

The comparison with the DHCAL and SDHCAL prototype data shows an advantage for low energies of the scintillator-tile calorimeter. However this effect could be explained by: the different sampling fraction of 5 mm scintillator versus 1.15 mm gas gap; a different threshold setting; the difference in the signal distributions (a Landau [21] versus a Polya function [22], which is very sensitive to high voltage variations); or the difference in the ionisation energy of the scintillator versus the gas mixture. A validated simulation of the RPC data would have the power to give answers to some of these open questions. First results for the DHCAL with minimal absorber [23] and the SDHCAL test beam data simulations [24] have been published within the CALICE collaboration, and the simulation of the Fe-DHCAL test beam data is ongoing.

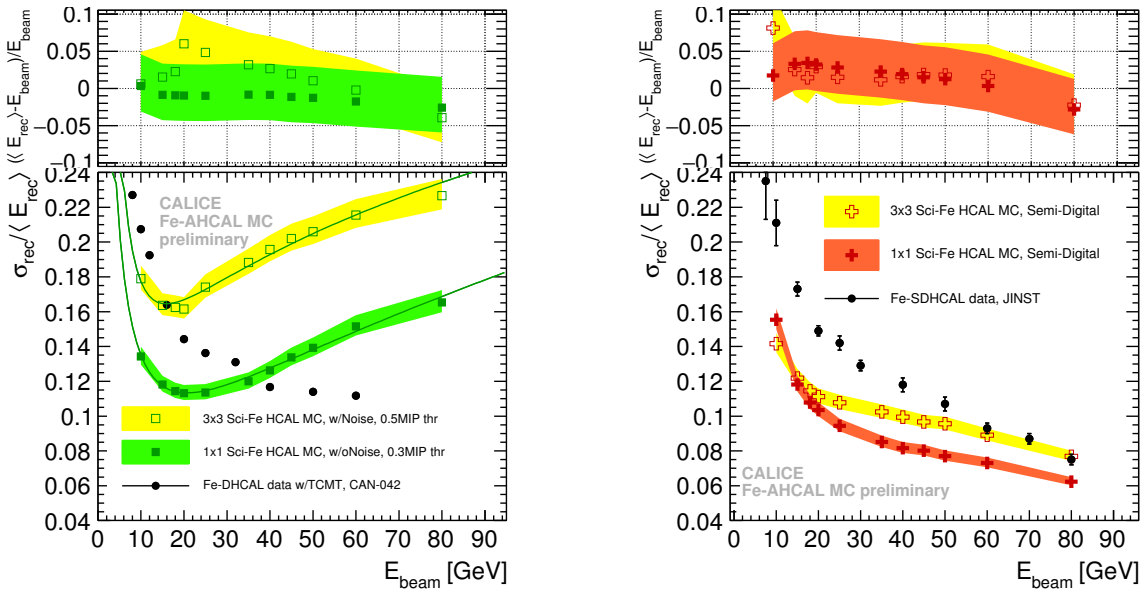

a) Digital Resolutions

b) Semi-Digital Resolutions

Figure 23: The digital and semi-digital energy resolutions of the FTFP_BERT simulations are shown as a function of beam energy for cell granularities of 1×1 and at most $3 \times 3\,\mathrm{cm}^2$. The results are compared to the test beam data of the DHCAL [7] and SDHCAL [8] prototypes. The plots on the top show the residuals to the beam energy with the bands indicating the systematic and statistical uncertainties. The purely statistical errors are smaller than the markers.

The main simulation-based results of these studies are summarised in Figure 24, which shows the energy resolutions for the semi-digital and software compensation reconstruction dependent on the Fe-AHCAL cell size for the simulations using the

FTFP_BERT physics list. This comparison reveals that the best energy resolution of the AHCAL with $3 \times 3\,\mathrm{cm}^2$ cells is reached using the software compensation algorithm, and therefore the analogue hit information is needed. For the $1 \times 1\,\mathrm{cm}^2$ AHCAL the hit information of 3 thresholds is sufficient. The resolution achieved by the AHCAL is similar when using software compensation algorithms for both the studied granularities (compare open and filled blue squares).

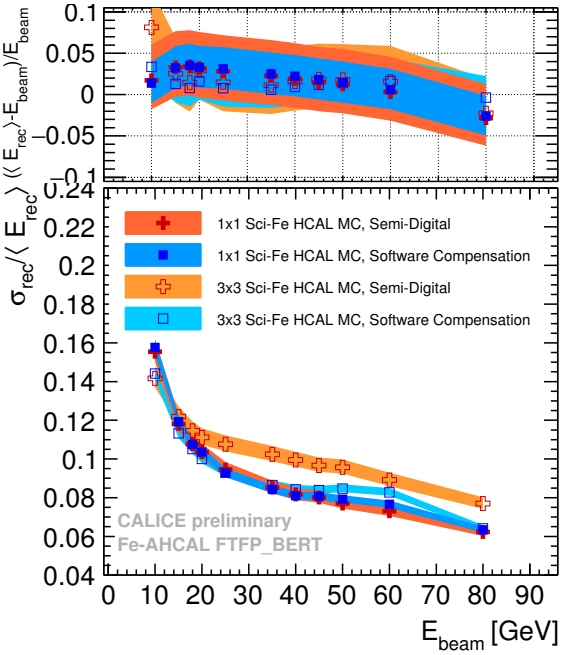

Figure 24: The resolutions of the semi-digital and software compensation energy reconstruction procedures of the FTFP_BERT simulations are shown as a function of beam energy for cell granularities of 1×1 and at most $3 \times 3\,\mathrm{cm}^2$. The plot on the top shows the residuals to the beam energy with the bands indicating the systematic and statistical uncertainties. The statistical errors are smaller than the markers.

7 Conclusions

Within the CALICE collaboration, several high granularity hadronic calorimeters have been developed and tested in test beams using large prototypes. Different energy reconstruction methods are used for the different prototypes, depending on their readout schemes. The signals measured by the analogue HCAL prototype can also be analysed with the reconstruction methods developed for the digital and the semi-digital HCAL, and thus allow a direct comparison of the reconstruction methods by applying them to the same data sample. Additionally, the new software compensation algorithm was developed. All methods are tested on pion test beam data collected in 2007 at CERN and on GEANT4 based simulations of that test beam setup, including the detector response. The validation of the simulation allowed a MC study of an AHCAL with $1 \times 1\,\mathrm{cm}^2$ granularity, which in turn allows the direct comparison between the different hadronic calorimeter prototypes.

Since all four reconstruction methods provide a reasonable linearity the results of the different energy resolutions can be compared. This comparison reveals that for the AHCAL with $3 \times 3\,\mathrm{cm}^2$ granularity, analogue hit information is needed to achieve the best possible resolution by applying the analogue software compensation algorithm. An AHCAL with $1 \times 1\,\mathrm{cm}^2$ granularity with the hit information extracted using 3 readout thresholds achieves, after an optimisation of the threshold values, an equal resolution as the $3 \times 3\,\mathrm{cm}^2$ AHCAL using the analogue software compensation algorithm.

For the optimisation of the International Large Detector (ILD) for the ILC, these results will have to be validated by implementing the reconstruction schemes into the Particle Flow algorithm.

References

[1] CALICE collaboration, CALICE Report to the Calorimeter R&D Review Panel
ILC-DET-2007-024, LC-DET-2007-007
arXiv:0707.1245

[2] CALICE collaboration, Calibration of the Scintillator Hadron Calorimeter of ILD
CALICE Analysis Note CAN-018

[3] CALICE collaboration, C. Adloff et al., Hadronic energy resolution of a highly granular scintillator-steel calorimeter using software compensation techniques
2012 JINST 7 P09017
doi:10.1088/1748-0221/7/09/P09017

[4] CALICE collaboration et al., Electromagnetic response of a highly granular hadronic calorimeter
2011 JINST 6 P04003
doi:10.1088/1748-0221/6/04/P04003

[5] C. Adams et al., Design, Construction and Commissioning of the Digital Hadron Calorimeter - DHCAL
arXiv:1603.01653

[6] B. Bilki, J. Butler, T. Cundiff, G. Drake, W. Haberichtera , E. Hazen, J. Hoff, S. Holm, A. Kreps, E. May, G. Mavromanolakis, E. Norbeck, D. Northacker, Y. Onel, J. Repond, D. Underwood, S. Wub and L. Xia, Calibration of a digital hadron calorimeter with muons
008 JINST 3 P05001

[7] B. Bilki on behalf of the CALICE collaboration, The DHCAL Results from Fermilab test beams: Calibration
CALICE Analysis Note CAN-042

[8] CALICE collaboration et al., First results of the CALICE SDHCAL technological prototype

2016 JINST 11 P04001
doi:10.1088/1748-0221/11/04/P04001

[9] C. Neubüser, Fe-DHCAL: Software compensation
CALICE Collaboration Meeting at ALCW 2015, KEK
19-24th April 2015
agenda.linearcollider.org/event/6557/session/0/contribution/251

[10] M. Chadeeva on behalf of the CALICE collaboration, Pion and proton showers in the CALICE scintillator-steel AHCAL: comparison of global observables
CALICE Analysis Note CAN-040

[11] CALICE collaboration et al., Validation of GEANT4 Monte Carlo models with a highly granular scintillator-steel hadron calorimeter
2013 JINST 8 P07005
doi:10.1088/1748-0221/8/07/P07005

[12] B. Lutz, Hadron Showers in a Highly Granular Calorimeter
DESY-THESIS-2010-048

[13] N. Feege, Low-energetic hadron interactions in a highly granular calorimeter
DESY-THESIS-2011-048

[14] D. Jeans, Recent developments in Linear Collider Calorimeter R&D
Linear Collider Workshop in Whistler, Canada
2-7 November 2015

[15] D. Boumediene on behalf of the CALICE collaboration, Response of the CALICE Si-W ECAL Physics Prototype to electrons
2009 J. Phys.: Conf. Ser. 160 012065
doi:10.1088/1742-6596/160/1/012065

[16] CALICE collaboration, C. Adloff et al., Construction and performance of a silicon photomultiplier/extruded scintillator tail-catcher and muon-tracker
2012 JINST 7 P04015
doi:10.1088/1748-0221/9/01/P01004

[17] M. Chefdeville, Off-line compensation of a SDHCAL, a Monte Carlo study
CALICE Collaboration Meeting in Hamburg,
20-22 March 2013
agenda.linearcollider.org/event/5947/session/4/contribution/6

[18] M. A. Thomson, Particle Flow Calorimetry and the PandoraPFA Algorithm
Nucl.Instrum.Meth.A611:25-40,2009
doi:10.1016/j.nima.2009.09.009

[19] C. Günther, Comparison of Iron and Tungsten Absorber Structures for an Analog Hadron Calorimeter
DESY-THESIS-2015-018

[20] C. Neubüser, K. Krüger on behalf of the CALICE collaboration, Analogue, Digital and Semi-Digital Energy Reconstruction in the CALICE AHCAL
CALICE Analysis Note CAN-049

[21] L. Landau, On the energy loss of fast particles by ionization
J.Phys.(USSR), vol. 8, pp. 201205, 1944

[22] M. Abbrescia et al., The simulation of resistive plate chambers in avalanche mode: charge spectra and efficiency
Nucl. Instr. and Meth. A 431,1999, p. 413

[23] CALICE collaboration et al., DHCAL with Minimal Absorber: Measurements with Positrons
JINST preprint
arXiv:1603.01652

[24] CALICE collaboration et al., Resistive Plate Chamber Digitiz ation in a Hadronic Shower Environment
JINST preprint
arXiv:1604.04550v1

Appendix

A ECAL Contribution to the Energy Reconstruction

Usually the ECAL contribution to the reconstructed energy is calculated by

$$\mathrm{E_{ECAL}} = \sum_{\mathrm{k}=1}^{3} \nu_{\mathrm{k}} \cdot \mathrm{M_{ECAL,k}} \tag{15}$$

with $\mathrm{M_{ECAL,k}}$ is the energy sum in the ECAL layers with in region k with sampling fraction ν_{k}. In this study, for the events with MIP-like tracks in the ECAL, the $\mathrm{E_{ECAL}}$ was reconstructed with an average conversion factor, taken from [3], of $\sum_{\mathrm{k}=1}^{3} \nu_{\mathrm{k}}/3 = 0.005906\,\mathrm{GeV/MIP}$. Thus the reconstructed energy is given by

$$\mathrm{E_{ECAL}} = 0.005906 \cdot \sum_{\mathrm{k}=1}^{3} \mathrm{M_{ECAL,k}}. \tag{16}$$

The resulting $\mathrm{E_{ECAL}}$ distribution for all selected pion events, with MIP like tracks in the ECAL, summed up over all energies is shown in Figure 25.
The mean value of the energy deposited in the ECAL, 0.3232 GeV, is used in the analysis.

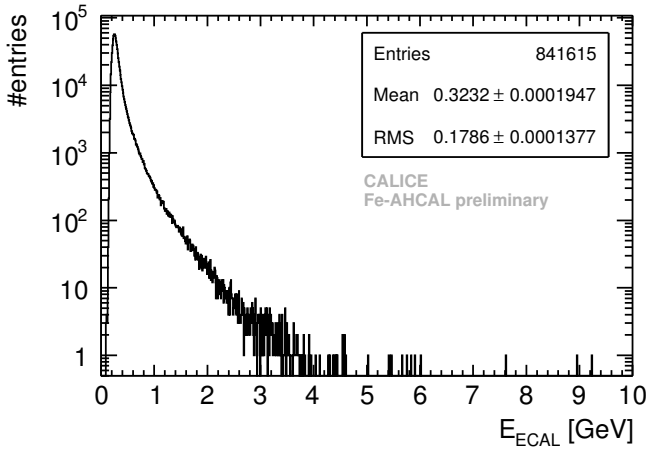

Figure 25: Distribution of the reconstructed energy in the ECAL for selected events with track in ECAL for all runs and energies.

B More Software Compensation Weights

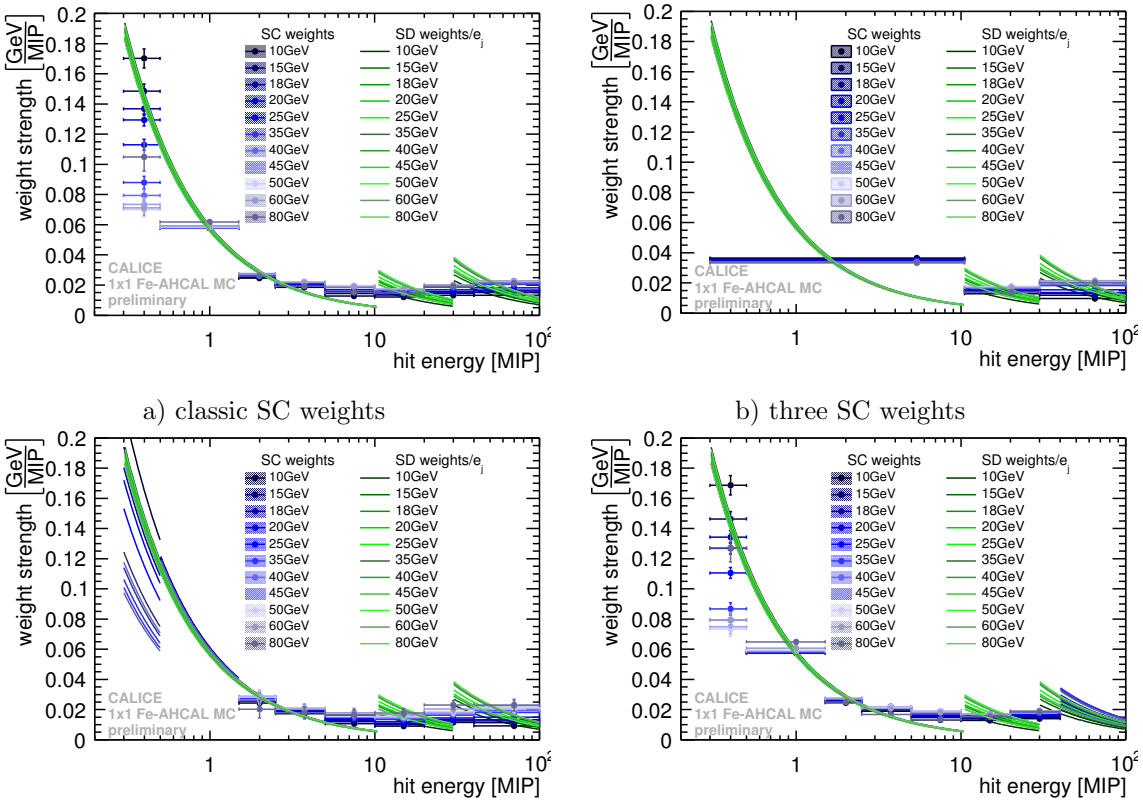

a) classic SC weights

b) three SC weights

c) two digital SC weights

d) digital highest SC weight

Figure 26: The weights used for the software compensation compared to the weights of the semi-digital energy reconstruction in the $1 \times 1\,\mathrm{cm}^2$ AHCAL FTFP_BERT simulation are shown as a function of the hit energy for the beam energies of 10-80 GeV. The software compensation weights are shown as blue bars/lines covering a certain hit energy range, the semi-digital weights are shown in green lines following a $1/e_j$ behaviour.